DOKUZ EYLÜL UNIVERSITY
GRADUATE SCHOOL OF NATURAL AND APPLIED SCIENCES

NUMERICAL INVESTIGATION OF A MAGNETIC REFRIGERATION SYSTEM FOR NEAR-ROOM TEMPERATURE APPLICATIONS

by
Tunahan AKIŞ

June, 2019
İZMİR

NUMERICAL INVESTIGATION OF A MAGNETIC REFRIGERATION SYSTEM FOR NEAR-ROOM TEMPERATURE APPLICATIONS

A Thesis Submitted to the
Graduate School of Natural and Applied Sciences of Dokuz Eylül University
In Partial Fulfillment of the Requirements for Master Degree in Mechanical Engineering, Thermodynamics Master Program

by

Tunahan AKIŞ

June, 2019
İZMİR

M.Sc. THESIS EXAMINATION RESULT FORM

We have read the thesis entitled **"NUMERICAL INVESTIGATION OF A MAGNETIC REFRIGERATION SYSTEM FOR NEAR-ROOM TEMPERATURE APPLICATIONS"** completed by **TUNAHAN AKIŞ** under supervision of **ASSOC. PROF. DR MEHMET AKİF EZAN** and **ASSOC. PROF. DR ORHAN EKREN** and we certify that in our opinion it is fully adequate, in scope and in quality, as a thesis for the degree of Master of Science.

EZAN

....

Assoc. Prof. Dr. Mehmet Akif EZAN

Supervisor

....

Assoc. Prof. Dr. Orhan EKREN

Supervisor

....

Assoc. Prof. Dr. Alpaslan TURGUT

Jury Member

....

Asst. Prof. Dr. Ahmet YILANCI

Jury Member

....

Asst. Prof. Dr. Levent BİLİR

Jury Member

Prof. Dr. Kadriye ERTEKİN

Director

Graduate School of Natural and Applied Sciences

ACKNOWLEDGEMENTS

I would like to thank Assoc. Prof. Dr. Mehmet Akif EZAN who did not deprive me of his deep knowledge and opinions, and to my second advisor Assoc. Prof. Dr. Orhan EKREN and his colleague Asst. Prof. Dr. Ahmet YILANCI, who has beneficial ideas and also improve my motivation. Also, I have to thank Assoc. Prof. Dr. Serdar ÇELİK and his collaborator MSc. Mechanical Engineer Erim YANIK who gives new ideas about a magnetocaloric regenerator.

I would also like to thank the Dokuz Eylül University Physics Department Statistical Physics Group, for their different perspectives and contributions to modeling the magnetocaloric effect.

I would also like to thank my auntie Nesime KANDIR and my mother Sıdıka KANDIR and rest of my lovely family who supports me about everything.

I would also like to thank my friend Mustafa ERÇELİK and my friend Cem KALKAN, for their contributions when the review and arrangement of this thesis at the control stage.

Tunahan AKIŞ

NUMERICAL INVESTIGATION OF A MAGNETIC REFRIGERATION SYSTEM FOR NEAR-ROOM TEMPERATURE APPLICATIONS

ABSTRACT

In this thesis, the magnetocaloric effect and engineering applications of magnetocaloric regenerator are examined numerically. Two different types of regenerators, namely, cylindrical and parallel plate regenerators, are considered. Each of them made of Gadolinium element, which is commonly used in magnetic cooling technology as a magnetocaloric material. Parallel plate regenerator consists of Gadolinium plates arranged parallel to each other. The cylindrical regenerator contains cylindrically shaped Gadolinium. Heat transfer fluid is driven with pistons in parallel plate regenerator, but cylindrical regenerator is using pumps for driving heat transfer fluid. Magnetocaloric effect (MCE) was obtained by Weiss's mean field theory, and also dimensionless MCE characteristics are determined with an alternative method, namely mean-field approximation. SIMPLE (Semi-Implicit Method for Pressure-Linked Equations) algorithm was used for the solution of continuity and conservation equations. Basically, the cycle duration, piston velocity, pressure difference value, utilization factor, and design ratio are selected parameters, and the most suitable operating conditions within these parameters are determined. MCE characteristics are obtained coherently with literature. The maximum temperature span is observed as 9.9 K for piston velocity 0.15 cm/s and 8.28 K for 1.2 s cycle duration for parallel plate regenerator and cylindrical regenerator, respectively. Furthermore, structural examination at cylindrical regenerator shows that smaller Gadolinium diameter increases maximum temperature span and temperature span is calculated as 8.85 K for 1.2 s cycle duration and 40 mm Gadolinium radius. In conclusion, the most important result is increasing cycle durations, and heat transfer fluid velocity has a negative effect on regenerator performance.

Keywords: Magnetic Refrigeration, Magnetic Regenerator, Mean Field Theory, Computational Fluid Dynamics

ODA SICAKLIĞI CİVARINDAKİ UYGULAMALAR İÇİN MANYETİK SOĞUTMA SİSTEMİNİN SAYISAL İNCELENMESİ

ÖZ

Bu tez çalışmasında, manyetokalorik etki ve manyetokalorik rejeneratörün mühendislik uygulamaları sayısal olarak irdelenmiştir. Silindirik ve paralel plaka olarak isimlendirilen iki farklı rejeneratör tipi irdelenmiştir. Bu yapılar, çoğunlukla manyetik soğutma teknolojisinde manyetokalorik malzeme olarak kullanılan Gadolinium elementi ile oluşturulmuştur. Paralel plaka rejeneratör birbirlerine paralel olarak düzenlenmiş Gadolinyum plakalarını içermektedir. Silindirik rejeneratör ise silindir olarak şekillendirilmiş Gadolinyum ile oluşturulmuştur. Manyetokalorik etki (MKE) Weiss ortalama alan teorisi ile hesaplanmıştır. Ayrıca MKE karakteristikleri alternatif bir metod olan ortalama alan yaklaşımı ile irdelenmiştir. Süreklilik ve korunum denklemleri SIMPLE algoritması ile çözümlenmiştir. Temel olarak, döngü süresi, piston hızı, basınç farkı değeri, düzeltme faktörü ve tasarım oranı parametreleri nümerik irdeleme için seçilmiştir. Elde edilen bulgularda, öncelikle MKE literatür ile doğrulanmıştır. Sırasıyla, paralel plaka ve silindirik rejeneratör için maksimum sıcaklık düşümleri 0,15 cm/s piston hızında 9,9 K ve 1,2 s döngü süresi için 8,28 K olarak tespit edilmiştir. Öte yandan, silindirik rejeneratördeki yapısal irdeleme rejeneratör performansını iyileştirmiş ve daha küçük Gadolinyum çapları, 1,2 s döngü süresi ve 40 mm Gadolinyum yarıçapı için 8,85 K sıcaklık düşümü sağlamıştır. En önemli bulgu ise, artan döngü süreleri ve ısı transfer akışkanı hızının, rejeneratör performasını olumsuz yönde etkilediğinin gözlenmesidir.

Anahtar Kelimeler: Manyetik Soğutma, Manyetik rejeneratör, Ortalama alan teorisi, Hesaplamalı akışkanlar dinamiği

CONTENTS

LIST OF FIGURES

Page

LIST OF TABLES

Page

CHAPTER ONE
INTRODUCTION

Increasing population density and evolving living standards increase the energy need throughout the world rapidly. This change in terms of heating and cooling applications (HVAC & R) is examined; it is seen that the consumption required to condition the space in parallel with the total energy consumption increases rapidly. The share of the amount of electricity used by HVAC & R systems in total consumption is 40%, 31%, and 15%, respectively, when Europe, the USA, and the entire world statistics are examined (Almeida, Fonseca, Falkner & Bertoldi, 2009; Aprea, Greco & Maiorino, 2016; Kusiak, Li & Tang, 2010). The conventional vapor compression refrigeration cycles penetrate the ozone layer due to the chlorofluorocarbon (CFC) and hydrofluorocarbon (HFCF) based fluids they contain. The use of these fluids was blocked by the protocol signed in Montreal in 1987 (Montreal, 1987). Furthermore, due to the rapidly increasing consumption of human beings, both the atmosphere and the earth's temperature have increased over the years. The change in temperature adversely affects the ecosystem, leading to climate change, limiting the habitats of different species and the extinction of living species.

Global Warming Potential (GWP) index is used to define the effect of greenhouse gases on global warming. Vapor compression refrigeration systems have a direct and indirect impact on global warming. Leakage of the refrigerant from the system components or to the external environment during service can be considered as a direct effect. The indirect impact is the use of a carbon-releasing power plant for the generation of electrical energy used by the cooling system compressor. The indirect impact is directly related to the coefficient of performance (COP) of the system (Aprea et al. 2016). Due to environmental concerns, studies on the development of environmentally friendly and innovative cooling systems such as thermoelectric, thermoacoustic, absorption/adsorption, elasto-caloric and magnetic cooling have increased notably in recent years (Qian et al., 2016). In alternative cooling systems, solid-state cooling technologies such as magnetocaloric and elasto-caloric are prominent (Goetzler, Guernsey, Young, Fuhrman & Abdelaziz, 2016). In these systems, solid-state materials are used instead of refrigerant, and no solid-liquid or liquid-gas phase transitions are observed in the conventional sense. For this reason, high-pressure line designs that are to be considered in conventional vapor compression systems or frequently encountered refrigerant leaks are not required in solid-state cooling applications. It is known that magnetic cooling applications have no adverse effect on the environment in terms of global warming and the ozone layer (Aprea et al., 2016). On the other hand, there are no compressors in vapor compression cycles in magnetic cooling systems. They can be theoretically more efficient than vapor compression refrigeration because they do not have compression and expansion stages (Engelbrecht et al., 2005). In addition, the moving parts in the system are reduced, and the noise generated during the operation of the compressor is eliminated in magnetic cooling. Magnetic cooling systems have the potential to reduce global warming and greenhouse gas emissions, as well as energy efficiency (Eriksen et al., 2015). Due to the environmental impacts and high-performance cooling potential, research and development activities related to magnetic cooling are carried out in different fields such as developing magnetocaloric materials, regenerator design, and design of magnet geometries.

1.1 Literature Investigation

After the discovery of magnetocaloric effect (MCE) by Weiss and Piccard (1917); it was started with refrigeration cycle recommendations to achieve over-low temperatures using the paramagnetic salt in the magnetic field (Yu et al., 2003). The first experiment on magnetic cooling was carried out by Giauque & MacDougall (1933) and cooling to temperatures below 1 K (Giauque & MacDougall, 1933). Nowadays, magnetic refrigeration is used to achieve low-temperatures. At the same time, near room temperature magnetic cooling applications have also been the subject of various researches in recent years as an option to meet the air conditioning needs. Research in magnetocaloric materials became prominent in the mid-1970s. As a result of the experiments carried out by Brown (1976), the near room temperature magnetic cooling system prototype has been created (7T magnetic field, 14 K temperature difference) (Brown, 1976). With the need for alternative cooling technologies, different research groups in recent years, especially in the US and European countries, have concentrated on the studies about magnetic cooling.

Magnetic cooling systems are mostly reciprocating and rotary types (Aprea, Greco, Maiorino & Masselli, 2015; Aprea et al., 2016; Lionte, Vasile & Siroux, 2015; Aprea, Greco, Maiorino, 2017; Lozano et al., 2013). Lozano et al. (2013) studied experimentally on a rotary active magnetic regenerator (AMR) and compared experiment results with numerical data. The system basically consists of a permanent magnet and porous regenerator, which has porosity value as 0.36. Regenerator rotates between permanent magnets with different angular velocities. In a similar study, Eriksen et al. (2015) study on reducing heat loses. In conclusion, temperature span and COP of the system observed as 10.2 K and 3.1, respectively. Velázquez, Estepa, Palacios & Burriel (2016) conducted a study about the effects of initial conditions on a magnetic cooling system near room temperature. System's magnet is selected as NdFeB, and Gd magnetocaloric material is used in the system. Results show that the prototype of the system performs 19.3 K temperature drop at the cold side of its regenerator. Aprea et al. (2015) present a 2D model of packing bed (or porous media) regenerator made for magnetic cooling system near room temperature. Numerical results are also compared experimental results of rotary type magnetic refrigeration system with permanent magnets. Both the model simulation and the experimental study were performed at a fixed fluid flow rate of 7.0 L/min, while the frequency and the temperature of the AMR cycle were altered between 1.08-1.79 Hz and 289-302 K, respectively. Finally, pressure, velocity, and temperature fields are calculated and validated with AMR's experimental results. In another study, Lionte et al. (2015) developed a transient 2D reciprocating AMR that operates near room temperature. AMR configuration has 31 gadolinium plates oriented as parallel in a stack. In addition, magnetic field density is varied from 0.0 to 1.1 T. The development of the temperature gradient along with the length of the regenerator, temperature span and 2D temperature distribution are represented and results validated with experimental results. Also, system performance is investigated as a function of temperature. The highest COP of system is determined as 3.0 at 0.18 displaced fluid ratio at a frequency of 0.50 Hz. Eriksen et al. (2016) represent 1D AMR model theoretically for investigating the effects of unbalanced flow on system performance. In the study, rotary multi-bed AMR with cylindrical and compartmentalized regenerator is used. They concluded that COP and cooling power of the regenerator decreases approximately by 50% and 30% respectively. Niknia et al. (2016), performed transient numerical analyses on a 1D AMR model with using gadolinium spheres. In parallel to the numerical analyses, they perform an experimental study for cross-validation. For modeling external losses, a simple resistance network is used. They concluded that the cooling power of regenerator is decreased with increasing the external losses. In the experiment, external loss coefficients are estimated in order to determine conductance's connection to the cold and hot side of the regenerator. Kamran et al. (2016), studied a microchannel regenerator numerically with a commercial CFD solver. Channel diameter is varied from 0.7 mm to 2.0 mm. Moreover, heat transfer fluid in the system is driven by a piston-cylinder mechanism in different mass flow rates. The numerical results showed that the cooling capacity of the regenerator is significantly affected by utilization, frequency of cycle, the diameter of the microchannel, and flowrate profile. In conclusion, at a magnetic field of 0.8 T, predicted maximum cooling capacity is about 22 W with corresponding utilization of 0.2, porosity and cycle frequency are 0.5 and 50 Hz, respectively. Also, with these results, they concluded that microchannel is 7% higher than parallel plate regenerator. Lei, Engelbrecht, Nielsen & Veje (2017) studied numerically on four different types of regenerators, namely parallel plate, microchannel, packed bed, and packed sphere. They studied on 1D models. Finally, they obtained maximum COP as 11.2 for the parallel plate matrix when hydraulic diameter, frequency were 0.15 mm and 3.7 Hz, respectively.

1.2 Motivation of Thesis

In this thesis, two different regenerator geometries are investigated numerically. Also, the evaluation of the magnetocaloric effect (MCE) is represented. Chapter two is focused on two numerical solution methods of MCE, one of them is Mean Field Theory, and the other one is Weiss Mean Field theory. Both of them are solved with numerical methods with developed algorithms by the author. Results of Weiss Mean Field Theory is validated with literature and represented. Chapter three is focused on parallel plate regenerator's energetic performances and hydrodynamical behaviors. 2D continuity, conservation, and energetic differential equations are solved numerically. MCE is integrated with the energy equation by using a user-defined function (UDF). The key parameters are selected as namely piston velocity, corresponding utilization factor, and fluid displacement ratio. In conclusion, temperature drop at cold side heat exchanger is represented regarding critical parameters. Chapter four is focused on cylindrical regenerator's hydrodynamic behavior and energetic performance characteristic. Firstly, the regenerator is investigated in hydrodynamical point of view then, energetic calculations are performed. MCE is integrated with the energy equation by using a UDF. UDF is developed in C programming media. Selected key parameters for cylindrical regenerator are cycle duration, the pressure difference between right and left side of the fluid channel, annulus gap ratio, and corresponding utilization factor. 2D axisymmetric continuity, conservation, and energy equation are solved numerically with a commercial CFD solver ANSYS-FLUENT. In literature, common approach for solving a magnetocaloric regenerator is defining MCE to energy equation as a source term. In this thesis, new algorithms that are different from literature for this coupling were developed. Also, it has been observed that these algorithms provided less computational time and much more accuracy for the behavior of MCE in regenerator's numerical domain. Also, An original regenerator type named cylindrical regenerator was developed in this work.

CHAPTER TWO
MODELING MAGNETOCALORIC EFFECT

The magnetocaloric effect has recently become one of the most studied research subjects in the fields of thermodynamics and statistical physics. The commonly used method, especially in engineering applications, is Weiss Mean Field theory. In this study, two methods are examined for calculating MCE named as *(i)* Mean Field Theory *(ii)* Weiss Mean Field Theory.

2.1 Mean Field Approximation

2.1.1 Magnetization of Material

The mean field approximation used in obtaining the MCE is the first basic tool to estimate the magnetic behavior of complex spin systems roughly. It is based on an average of total spin-spin interaction average principle. The total energy of the system is given by the Hamiltonian expression (Strecka & Jascur, 2015)

$$E = -J \sum_{<i,j>} S_i S_j - g\mu_b h \sum_{i=1}^{N} S_i \qquad (2.1)$$

where S_i represents spin i 7/2-atom at knitting point. The first sum in Equation 2.1 is the sum over all nearest neighbor spin pairs and the other sum is the summation of all over a spin system consisting of N spins. J represents the spin-spin interaction constant between nearest neighbor two spins and h represents the magnetic flux density applied normal direction to spin system. g is Landau Factor and μ_b is Bohr Magneton. The mean field approach neglects all local fluctuations in spin-spin correlations. Purpose of this calculation is to validate the material's magnetocaloric behavior. So, J is neglected by scaling out magnetic flux density input and temperature (Equation 2.2)

$$T = \frac{k_b t}{J} \qquad\qquad H = \frac{h}{J} \tag{2.2}$$

The Gibbs-Bogoliubov variational principle is used for the determination of MCE characteristics. Unlike many alternative formulas, it is based on the following inequality (Equation 2.3) (Strecka & Jascur, 2015).

$$F \leq \Phi \equiv F_0 + < E - E_0 >_0 \tag{2.3}$$

where F is quantitative real free energy and E is real Hamiltonian of the system. F_0 and E_0 are the trial free energy and trial Hamiltonian expressions, respectively. $< \cdots >_0$ the expression is the average canonical density of Hamiltonian. Φ represents the upper limit for the actual free energy of variational free energy. Rewriting the initial trial Hamiltonian with Equation 2.4 as follows

$$E_0 = -\gamma \sum_{k=1}^{N} S_k \tag{2.4}$$

where γ is the variational parameter which can be calculated by minimizing variational free energy Φ.

The partition function of the system is defined with Equation 2.5.

$$Z_0 = \sum_{\{S_k\}} e^{-\beta H_0} = \prod_{k=1}^{N} \sum_{S_k} e^{(\beta \gamma S_k)} \tag{2.5}$$

Furthermore, the system's free energy calculated with Equation 2.6.

$$F_0 = -k_b T ln Z_0 \tag{2.6}$$

System's total magnetization is given by Equation 2.7;

$$m_0 = -\frac{1}{N}\frac{\partial F_0}{\partial \gamma} \tag{2.7}$$

The spin-spin interaction correlations with mean field theory approach can be written by Equation 2.8.

$$< S_i S_j >_0 = < S_i >_0 < S_j >_0 = m_0^2 \tag{2.8}$$

The actual free energy and actual magnetization of the system are calculated by replacing the γ variational parameter after minimizing Φ variational parameter obtained.

2.1.2 Calculating Magnetocaloric Effect

It can be said that in a magnetocaloric material, the magnetocaloric effect is a result of three entropy genesis (Tishin, 1990). These are Magnetic Entropy, Lattice Entropy, and Electron Entropy as written as Equation 2.9

$$S_{tot}(T,H) = S_{magnetic}(T,H) + S_{lattice}(T,H) + S_{electron}(T,H) \tag{2.9}$$

The first term on the right-hand side of the Equation 2.9 is magnetic entropy contribution to total entropy calculated as Equation 2.10

$$S_{magnetic}(T,H) = -\left(\frac{\partial F}{\partial T}\right)_{m,H} \tag{2.10}$$

Also, the second term is lattice contribution given with Equation (2.11) (Tishin, 1990)

$$S_{lattice}(T,H) = \frac{R_u}{M_m}\left(-3\ln\left(1 - e^{-\frac{T_{debye}}{T}}\right) + 12\left(\frac{T}{T_{Debye}}\right)^3 + \int_{x=0}^{T_{debye}/T} \frac{x^3}{e^x - 1}\,dx\right) \tag{2.11}$$

The third term is the electron entropy contribution. This contribution can be neglected according to its value compared other two contributions (Tishin, 1990). Heat capacity in magnetocaloric material depends on both temperature and magnetic flux density. The calculation of heat capacity is given with Equation (2.12)

$$C = T\left(\frac{\partial S_{tot}}{\partial T}\right)_H \tag{2.12}$$

After magnetization and demagnetization processes, magnetocaloric material shows adiabatic temperature change and its magnetization entropy increases with both its temperature and magnetic flux density. The adiabatic temperature change of the process is calculated by Equation (2.13), thus magnetization entropy by both temperature and magnetic field density are calculated by Equation (2.14).

$$\Delta T_{ad} = -\int \frac{T}{C}\left(\frac{\partial m}{\partial T}\right) dH \tag{2.13}$$

$$\Delta S_m = \int \left(\frac{\partial m}{\partial T}\right) dH \tag{2.14}$$

2.1.3 Results of Mean Field Approximation

General magnetic behavior of magnetocaloric materials and scaled results are represented in this section. Note that every magnetocaloric material has a spin-spin interaction constant for itself. This result will be respectful when this constant taken into account.

All integrals are solved by numerically with Simpson's integral, and derivative terms are also solved numerically by high order (fourth-level) methods. In Figure 2.1(a), the critical dimensionless temperature is determined as 64.1 in the absence of the magnetic field. The system’s behavior is ferromagnetic under determined critical temperature. Higher than the critical temperature, the system’s magnetic behavior is observed as paramagnetic. This means that the magnetic phase transition from ferromagnetic to paramagnetic phase is not observed with an increasing magnetic field. As can be seen in Figure 2.1(b), it is consistent with iso-thermal cases under varying magnetic flux density values.

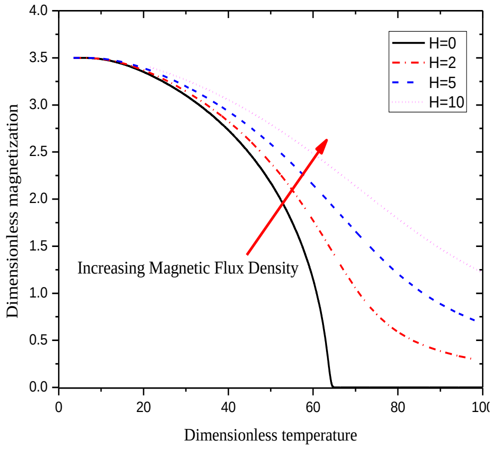

(a)

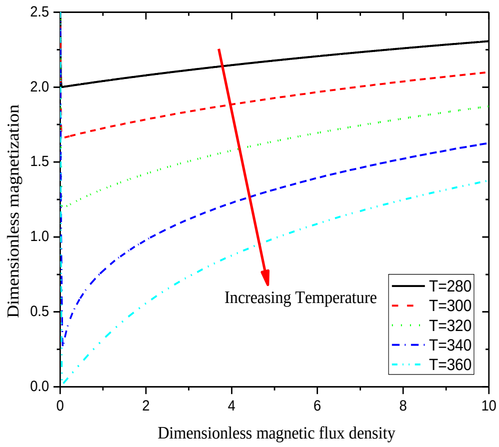

(b)

Figure 2.1 Magnetization of the system (a) by temperature (b) by magnetic flux density

The magnetic entropy of the system increases with advancing temperature, as shown in Figure 2.2. When the magnetic field removed, it shows breaking at the critical temperature, if magnetic flux density on the system increases entropy behavior shows nonlinear behavior beyond critical temperature. This behavior is also consistent for a magnetocaloric system.

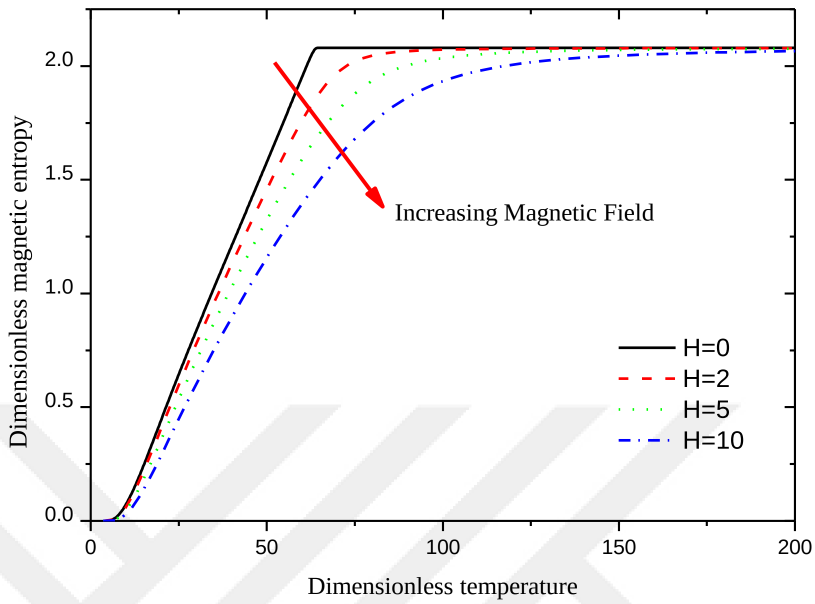

Figure 2.2 Magnetic entropy by increasing temperature

Dimensionless heat capacity is represented in Figure 2.3. In the absence of magnetic field, material’s heat capacity shows a discontinuity at the critical temperature; there is a sudden drop after that temperature, heat capacity no more shows a significant difference. Smoothing at curves is observed with advancing magnetic flux density around critical temperature, unlike the first situation, there are changes by temperature after critical temperature, this is also consistent for a magnetocaloric material behavior with advancing temperature and magnetic field.

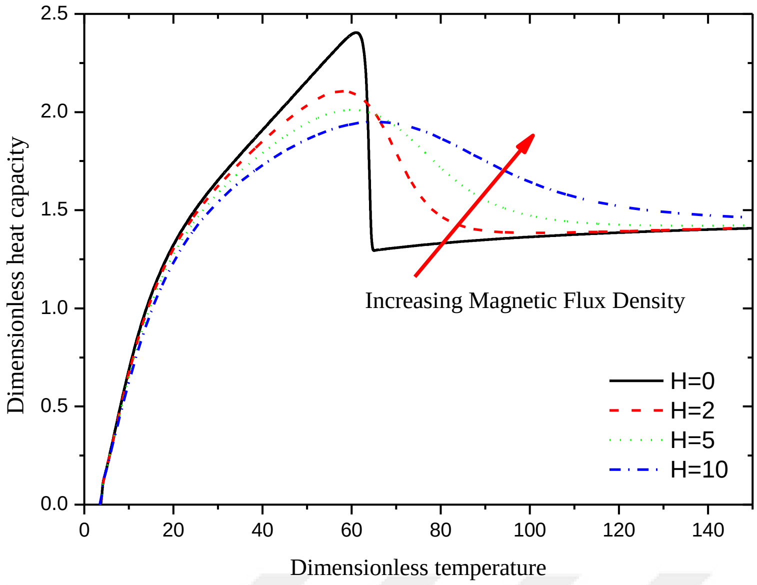

Figure 2.3 Heat capacity by increasing temperature

In Figure 2.4, magnetic entropy variations are represented. Total magnetic entropy change increases with advancing magnetic flux density. The maximum values are observed near the critical temperature; it is also consistent for a magnetocaloric material's behavior.

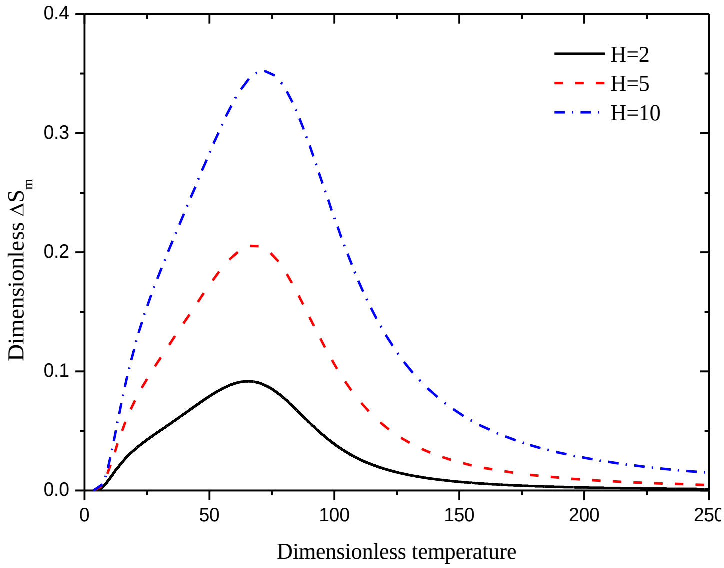

Figure 2.4 Entropy change by increasing temperature

2.2 Weiss Mean Field Theory

The phenomena of magnetocaloric effect (MCE) is known as a warming and cooling effect of a material which influenced with dynamic magnetic field density. From the side of engineering applications, this effect calculated and integrated with energy equation as a source term in W/m^3. In many cases in engineering, common MCE calculations are performed with Weiss Mean Field theory. MCE calculation is defined in Equation 2.15.

$$MCE = \rho c \left(\frac{\partial T}{\partial B}\right)_s \frac{\partial B}{\partial t} \tag{2.15}$$

where B is an external magnetic field (T), t is magnetization time (s), ρ is material density (kg/m^3), c (J/kg-K) is material heat capacity, T is material temperature (K). Because of the $\frac{\partial B}{\partial t}$ the term is dependent on magnetic field change by time, this term is a boundary condition for numerical simulations. On the other hand, for both solving $\frac{\partial B}{\partial t}$ term and calculating adiabatic temperature change temperature in material, Equation 2.16 is used (Tishin, 1990)

$$\left(\frac{\partial T}{\partial B}\right)_s = \left(\frac{\Delta T_{ad}(B,T)}{\partial B}\right)_s \tag{2.16}$$

Adiabatic temperature change is a function of both temperature and magnetic field density, and it is described by total entropy change of material by using Maxwell equations (Equation 2.17)

$$\Delta T_{ad}\,(B,T) = \frac{T}{c(B,T)}\, S_{total}(B,T) \tag{2.17}$$

Total entropy change calculations were described in the previous Chapter. In this method, magnetic entropy is calculated by an implicit function called Brillion function defined by Equation 2.18 (Tishin, 1990)

$$B_j(x) = \frac{2J+1}{2J}\coth\left(\frac{2J+1}{2J}\right) - \frac{1}{2J}\coth\left(\frac{x}{2J}\right) \tag{2.18}$$

where J is the total angular momentum of the spin system. Also, x independent variable is given by Equation 2.19

$$x = \frac{g_j \mu_b J B}{KT} + \frac{3T_{curie} J B_j(x)}{T(J+1)} \tag{2.19}$$

where g_j symbolizes spectroscopic factor, μ_b represents Bohr magneton, K is Boltzmann constant T_{Curie} reveals the Curie temperature of the material. In this thesis, Gadolinium is used as magnetocaloric material for all numerical simulations. Magnetic properties of the Gadolinium is given in Table 2.1.

Table 2.1 Magnetic Properties of Gadolinium

Property Name	**Unit**	**Value**
g_j	-	2
J	-	3.5
T_{Curie}	K	293
T_{Debye}	K	184
M_m	kg/mol	0.157

2.2.1 Results of Weiss Mean Field Theory

By solving Equations 2.18 and 2.19 iteratively, the magnetic entropy can be evaluated. In Figure 2.5, the current results are compared with the literature (Bouchekera &Nahas, 2012). In Figure 2.5, solid lines represent the calculated data, and the scatters represent literature data. The same behavior with mean field theory can be seen in these results. Beyond Gadolinium's critical temperature (293 K) same discontinuity at heat capacity and the peak value of adiabatic temperature change represented in Figure 2.5(b).

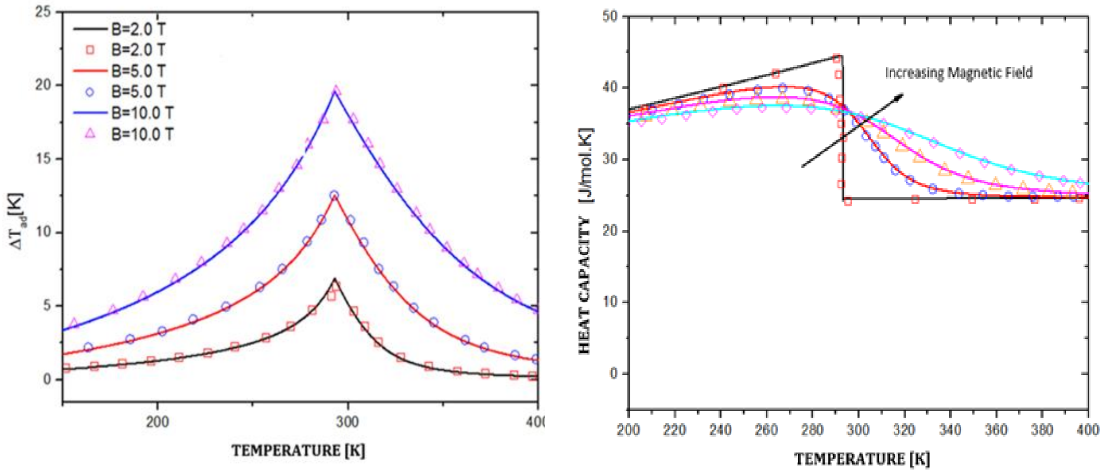

(a) (b)

Figure 2.5 Results of Weiss Mean Field Theory (a) Adiabatic Temperature Change (b) Heat Capacity

2.3 Multiphysics Structure of CFD Solver

In this thesis, two kinds of magnetocaloric regenerators are examined numerically. In this work, the MCE source term is defined with User Defined Functions (UDF). UDF algorithm is represented Figure 2.6. Asymmetric Double Sigmoidal method is implemented as the Curve fitting method. Fitted curves are represented in Figure 2.7.

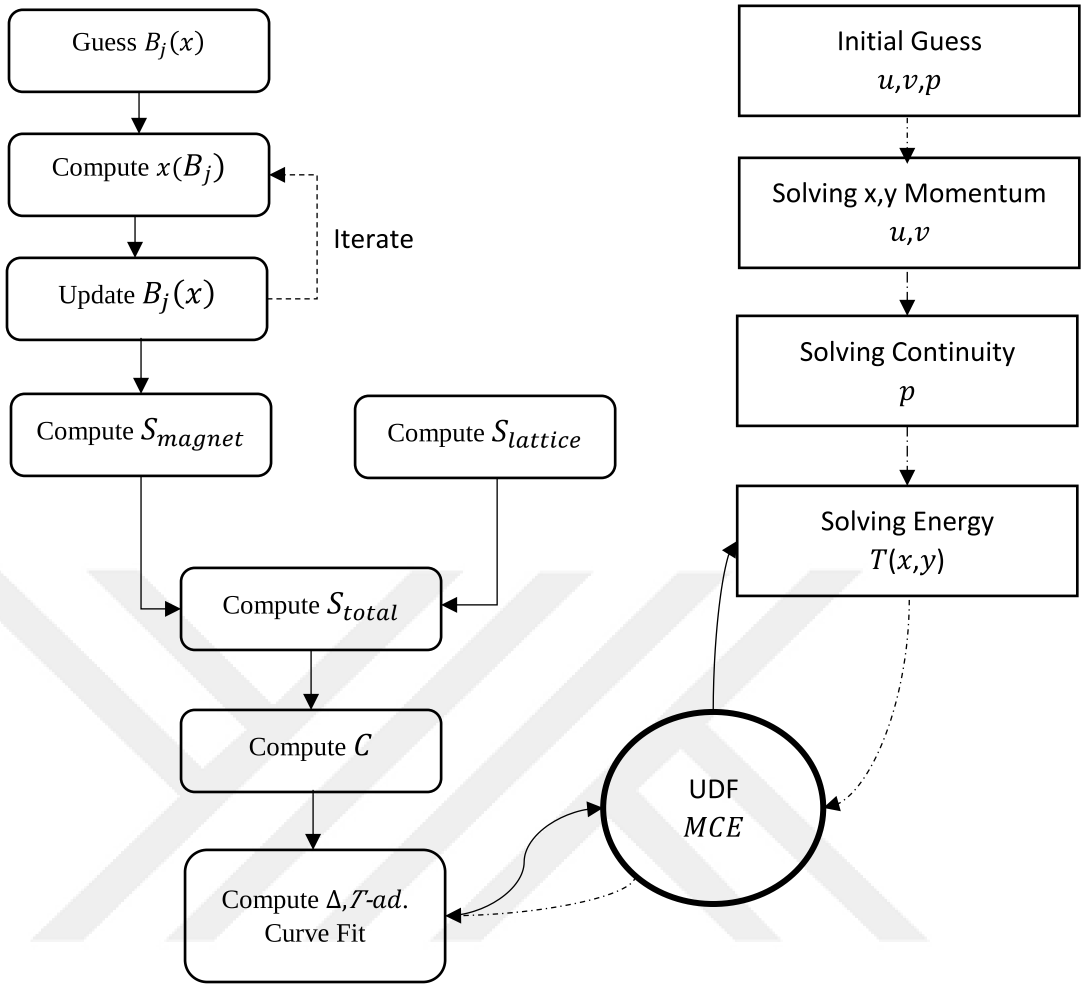

Figure 2.6 UDF Algorithm

In Equation 2.20 y_0, x_c, A, w_1, w_2, and w_3 are fitted curve constants which are given in Table 2.2. Constant values depend on advancing the magnetic field which varies between 0.4 T – 1.0 T.

$$\Delta T_{ad}(T) = y_0 + A\left(\frac{1}{1+\exp\left(\frac{-\left[T-x_c+\frac{w_1}{2}\right]}{w_2}\right)}\right)\left(-\frac{1}{1+\exp\left(\frac{-\left[T-x_c+\frac{w_1}{2}\right]}{w_3}\right)}\right) \tag{2.20}$$

Table 2.2 Fit Curve Constants

B[T]	y_0	x_c	A	w_1	w_2	w_3	***Adj. R²***
0.4	0.35098	296.37021	5.19801	3.98E-20	8.01642	2.22601	0.97464
0.5	0.48406	296.48996	6.04155	2.56E-25	8.1523	2.46752	0.97633
0.6	0.63254	296.56978	6.76632	3.071E-12	8.2295	2.65479	0.97755
0.7	0.78887	296.61556	7.41662	2.09E-12	8.26777	2.81916	0.97848
0.8	0.95399	296.63928	7.99105	2.14E-13	8.2759	2.95637	0.97923
0.9	1.04641	296.65687	8.80595	1.05E-38	8.42666	3.23519	0.98033
1.0	1.29913	296.63718	8.97968	1.17E-30	8.23707	3.18538	0.9804

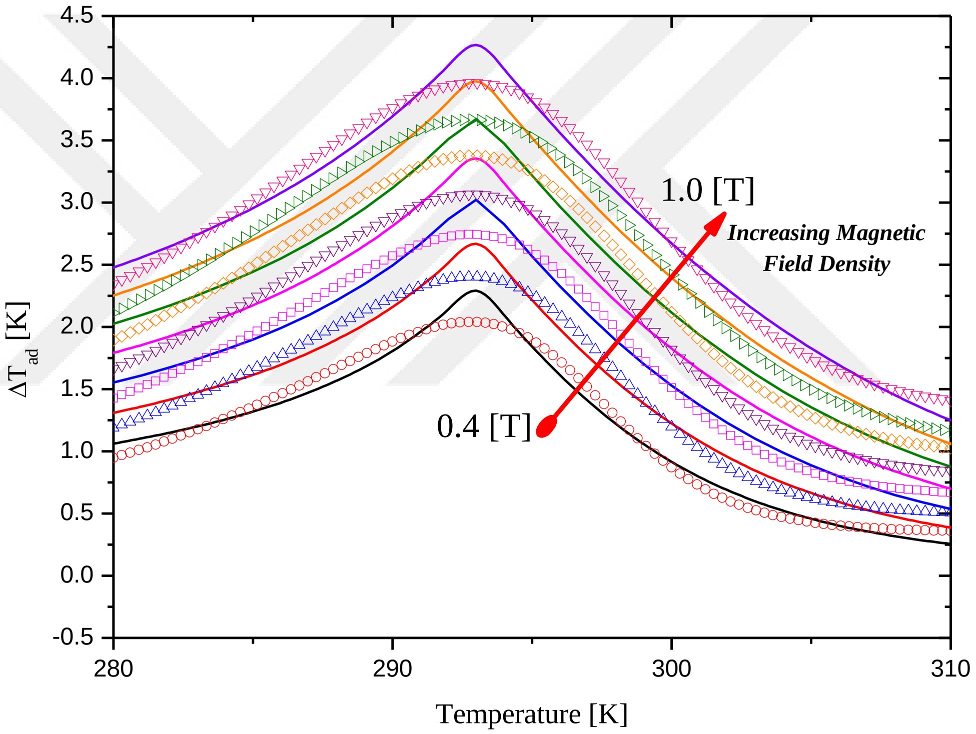

Figure 2.7 Fitted adiabatic temperature change curves by cell temperature

CHAPTER THREE
PARALLEL PLATE REGENERATOR

3.1 Definition of Problem

In this chapter, parallel plate regenerator built with parallel gadolinium plates examined numerically. Physical model of the system represented in Figure 3.1.

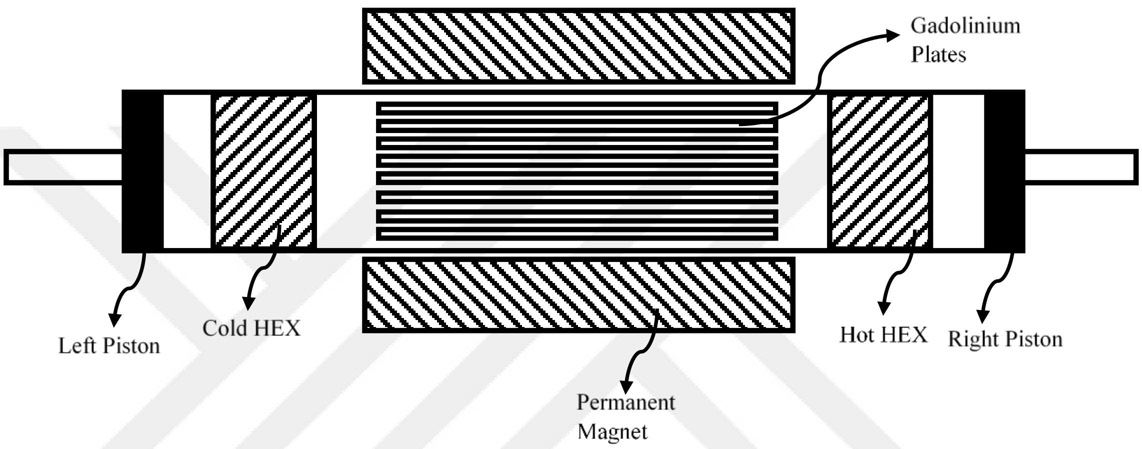

Figure 3.1 Physical model of parallel plate regenerator

The model consists of *(i)* cylinders, *(ii)* pistons, *(iii)* gadolinium plates (as magnetocaloric material), *(iv)* permanent magnets, *(v)* hot heat exchanger, and *(iv)* cold heat exchanger. In this thesis, gadolinium is used as the magnetocaloric material because its Curie temperature is near room temperature (T_{Curie} = 293 K). There are two pistons driven linearly at both ends of the cylinder. Parallel plate-shaped gadolinium plates are positioned in the middle of the cylinder. There are copper heat exchangers at both ends of the magnetocaloric bed. The system‘s geometric parameters obtained from the literature (Petersen, 2017). The most important component of the system is the magnetocaloric bed (or regenerator), and regenerator’s all parameters are detailed in this section.

The system is driven by a linear piston mechanism which has a constant velocity. When magnetocaloric material is at the among of the magnets, this step is named as magnetization and material is magnetized at this time. In this step, magnetocaloric material is getting warmer in a short time. At the end of pre-described magnetization, step pistons move right side, thus heat transfer fluid flows through a heat exchanger called hot heat exchanger. This flow duration named hot blow and during this step warmed magnetocaloric material is exposed forced convection which cools down magnetocaloric material. Rejected heat from magnetocaloric material is transferred to heat transfer fluid. After that, the magnetic field is removed from the regenerator and material cools down instantly. This step is named as demagnetization. After that time, pistons move through the left side, and cold blow occurs.

For determining the system performance quickly, there is a geometric reduction, which is explained in Figure 3.2. As can be seen in Figure 3.2, one repeating module which consists of a gadolinium plate, flow channel, heat exchangers, and pistons are modeled instead of the whole magnetocaloric bed. This reduction also clarifies the boundary conditions of the physical model. Symmetrical boundary conditions are applied to regenerator geometry, flow channel, and heat exchangers. Finally, the reduced model is clarified with this reduction. Figure 3.3 shows the reduced model and boundary conditions. Geometric inputs are given in Table 3.1.

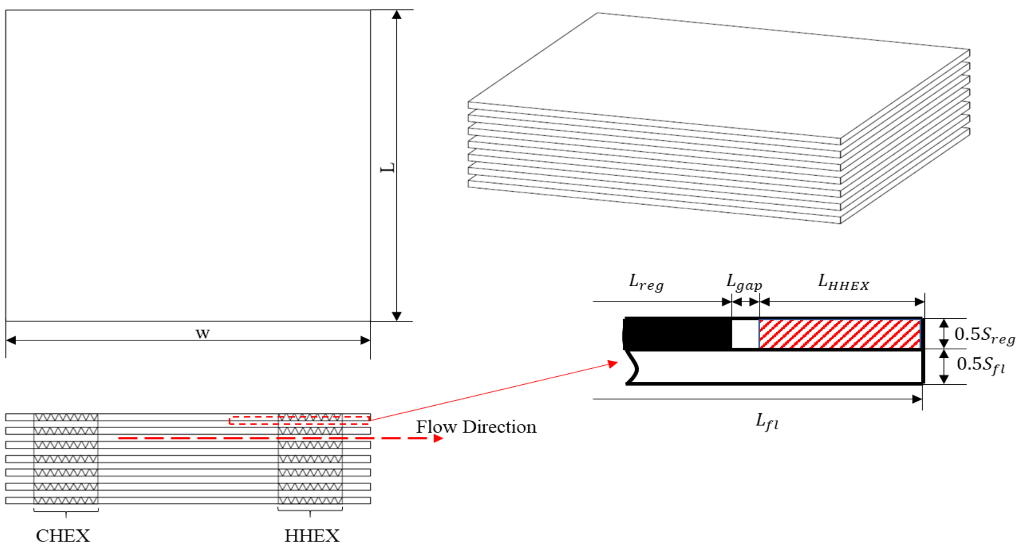

Figure 3.2 Parallel plate regenerator geometry

Table 3.1 Geometric values of magnetic regenerator (Petersen, 2017)

Part Name	Geometric Value	Unit
Regenerator (L_{reg})	5	cm
Heat Exchangers ($L_{H/CHEX}$)	2	cm
Fluid Channel (L_{fl})	16	cm
Insulation Gap (L_{gap})	1	cm
Fluid Channel Height (S_{fl})	5	mm
Regenerator Height (S_{reg})	5	mm

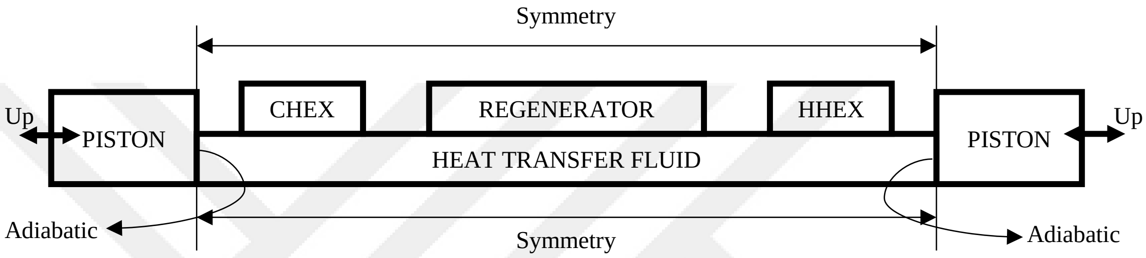

Figure 3.3 Reduced computational model of parallel plate regenerator

In this study, the performance of the magnetic regenerator was investigated without any load. For this reason, the upper surface of cold heat exchanger (CHEX) is defined as adiabatic. On the other hand, hot heat exchanger (HHEX) temperature is kept constant (T_{HHEX} = 298 K). Symmetric conditions that are given in Figure 3.3 are defined for reducing mesh number, and computational time, also regenerator's geometry allows this reduction, which can be seen in Figure 3.2.

The magnetic cooling system consists of four periods, which are magnetization, cold flow, demagnetization, and hot flow periods similar to the problem described by Petersen (2007). These four periods are defined in Figure 3.4. Cycle durations selected as τ_1=2 s (*magnetization*), τ_2 =1 s (*hot blow*), τ_3=2 s (*demagnetization*), and τ_1=1 s (*cold blow*), so the total cycle duration is 6 s.

The magnetic field intensity of the magnet applied to the material is changed instantly from B = 0.0 T, as the minimum value, to B = 1.0 T, as the maximum value.

In addition, the thermophysical properties of the material used in the study are given in Table 3.2

Uniform velocity profiles are defined to the pistons; thus, pistons move through the left side or the right side. In this work, this substitution is named piston stroke, which is the key parameter for the obtaining performance of this magnetocaloric system.

Table 3.2 Thermophysical properties of used materials in the regenerator (Petersen, 2017)

Material	C_p **[Jkg^{-1}K^{-1}]**	k **[Wm^{-1}K^{-1}]**	ρ **[kgm^{-3}]**	μ **[kgm^{-1}s^{-1}]**
Gadolinium	235	10.5	7900	-
Copper	385	401	8933	-
Water	4183	0.595	997	8.91E-4

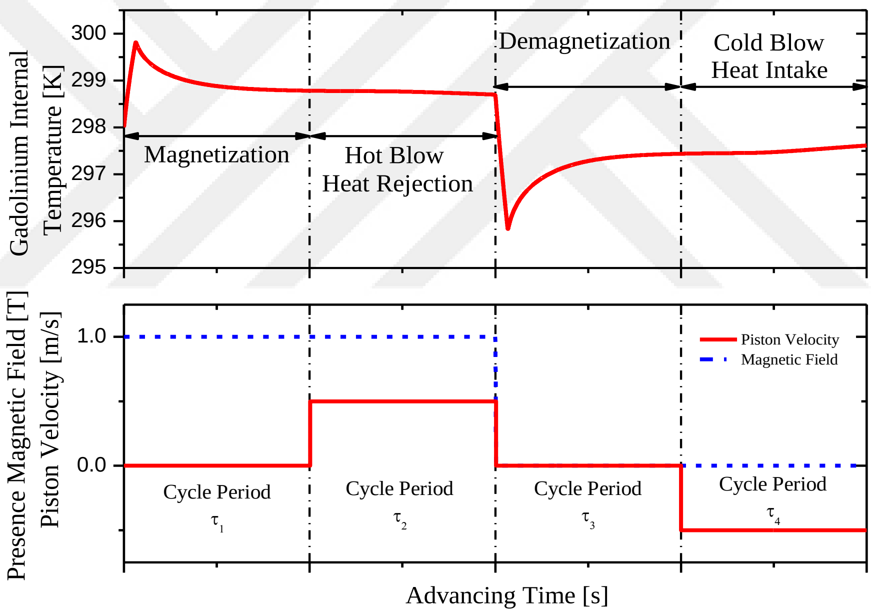

Figure 3.4 Parallel plate regenerator operating conditions

As magnetocaloric material, gadolinium was preferred because it is suitable for cooling applications at room temperature. The specific heat of the gadolinium is calculated based on the temperature, and the intensity of the magnetic field applied. The calculation details are given in Chapter 2.

3.2 Dynamic Mesh Structure of Model

In the model, the motion of the heat transfer fluid was carried out by a dynamic mesh structure. The dynamic mesh algorithm is implemented by ANSYS-FLUENT's "Layering" algorithm. The main point to consider in the layering algorithm is the size of the time step. Otherwise, the algorithm will not work in the mesh will be seen in the warp. Two parameters, collapse, and split factor are essential in the layering algorithm. If the cells in Layer-1 are expanding, the cell heights are allowed to increase considering the following criteria

$$h_{min} > (1 + \alpha_s)h_{ideal} \tag{3.1}$$

where h_{min} is the minimum cell height of cell Layer-1 h_{ideal} is the ideal cell height, and α_s is the layer split factor. These layers are represented in Figure 3.5.

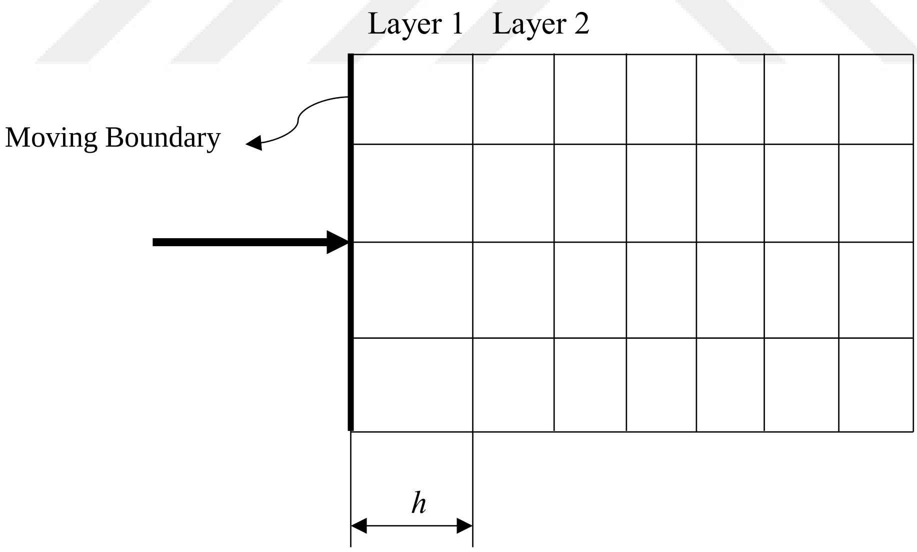

Figure 3.5 Dynamic layering

Note that ANSYS-FLUENT allows defining h_{ideal} as either a constant value or a value that varies as a function of time or crank angle. When the condition in Equation 3.1 is met, the cells are split based on the specified layering option. This option can be height based or ratio based.

If the cells in Layer-1 are being compressed, they can be compressed according to the following condition,

$$h_{min} < \alpha_c h_{ideal} \tag{3.2}$$

where α_c is the layer collapse factor. When this condition is met, the compressed layer of cells is merged into the layer of cells above the compressed layer; i.e., the cells in Layer-1 are merged with those in Layer-2. Mesh number information in this study is given with Table 3.3. The number of mesh information is taken from the literature (Petersen et. al., 2007).

Table 3.3 Mesh numbers of regenerator parts

Part	Coarse Grid	Normal Grid	Fine Grid
Regenerator	30x6	50x10	75x15
Heat Exchangers	10x6	20x10	30x15
Fluid Channel	215x15	320x20	480x30

3.3 Solution Method

The transient model is used for the solution. The numerical model is developed with a commercial finite volume solver, ANSYS-FLUENT. Some assumptions are considered in the numerical model:

- Heat transfer fluid is incompressible.
- Radiative effects with ambient are neglected, only convective and conductive heat transfer mechanisms are effective.
- Thermophysical properties of heat transfer fluid are constant.
- Flow is laminar.
- The magnetic field inside the solid domain is uniform.

With these assumptions, 2D governing equations can be written as below for the fluid domain

Continuity equation is given with Equation 3.3.

$$\frac{\partial u}{\partial y} + \frac{\partial v}{\partial y} = 0 \tag{3.3}$$

x and y momentum equations are given Equation 3.4 and Equation 3.5, respectively.

$$\begin{aligned} \frac{\partial}{\partial t}(\rho u) + \frac{\partial}{\partial x}(\rho uu) + \frac{\partial}{\partial y}(\rho vu) \\ = -\frac{\partial p}{\partial x} + \frac{\partial}{\partial x}\left[\frac{\partial}{\partial x}(\mu u)\right] + \left[\frac{\partial}{\partial y}(\mu u)\right] \end{aligned} \tag{3.4}$$

$$\begin{aligned} \frac{\partial}{\partial t}(\rho v) + \frac{\partial}{\partial x}(\rho uv) + \frac{\partial}{\partial y}(\rho vv) \\ = -\frac{\partial p}{\partial y} + \frac{\partial}{\partial x}\left[\frac{\partial}{\partial x}(\mu v)\right] + \frac{\partial}{\partial y}\left[\frac{\partial}{\partial y}(\mu v)\right] \end{aligned} \tag{3.5}$$

The energy equation is given by Equation (3.6).

$$\begin{aligned} \frac{\partial}{\partial t}(\rho cT) + \frac{\partial}{\partial x}(\rho ucT) + \frac{\partial}{\partial y}(\rho vcT) \\ = \frac{\partial}{\partial x}\left[\frac{\partial}{\partial x}(kT)\right] + \frac{\partial}{\partial y}\left[\frac{\partial}{\partial y}(kT)\right] \end{aligned} \tag{3.6}$$

For solid domain, energy equation can be stated as Equation (3.7)

$$\frac{\partial}{\partial \mathrm{t}}(\mathrm{\rho cT}) = \frac{\partial}{\partial \mathrm{x}}\left[\frac{\partial}{\partial \mathrm{x}}(kT)\right] + \frac{\partial}{\partial y}\left[\frac{\partial}{\partial y}(kt)\right] + MCE \tag{3.7}$$

The second-order upwind scheme is implemented for the discretization of convective terms and energy equation. Continuity and momentum equations are solved with Semi-Implicit Method for Pressure-Linked Equations (SIMPLE) algorithm.

The calculation procedure of the MCE term is given in Chapter-2. MCE term is integrated with energy equation as a volumetric heat source (Wm^{-3}) and is a function of cell temperature. This integration is completed with a user-defined function (UDF). UDF algorithm is explained in detail in Section-2.3. UDF code is developed C programming language to incorporate the MCE term into the energy equation, also UDF is capable of calculating the magnetocaloric material's heat capacity.

Initially, the system is at the near room temperature (T_{amb} = 25°C), and heat transfer fluid is stagnant ($u=v=0$). Time step size is defined as 0.05 s, and the convergence criteria for all of governing equations are set to be 10^{-6}.

3.4 Results of Parallel Plate Regenerator

3.3.1 Hydrodynamic Considerations

The flow between two fixed walls is similar to the Pousiulle flow. Full development in velocity profile analysis is presented in Figure 3.6 with symmetric boundary condition.

As is known, if the fully developed velocity profile is examined in a Poiseuille flow between two parallel plates, the maximum velocity will be 1.5 times of the mean inlet velocity. If this theoretical framework is considered, the accuracy of the solution and the validation of the model can be seen in the preliminary hydrodynamic results as represented in Figure 3.6.

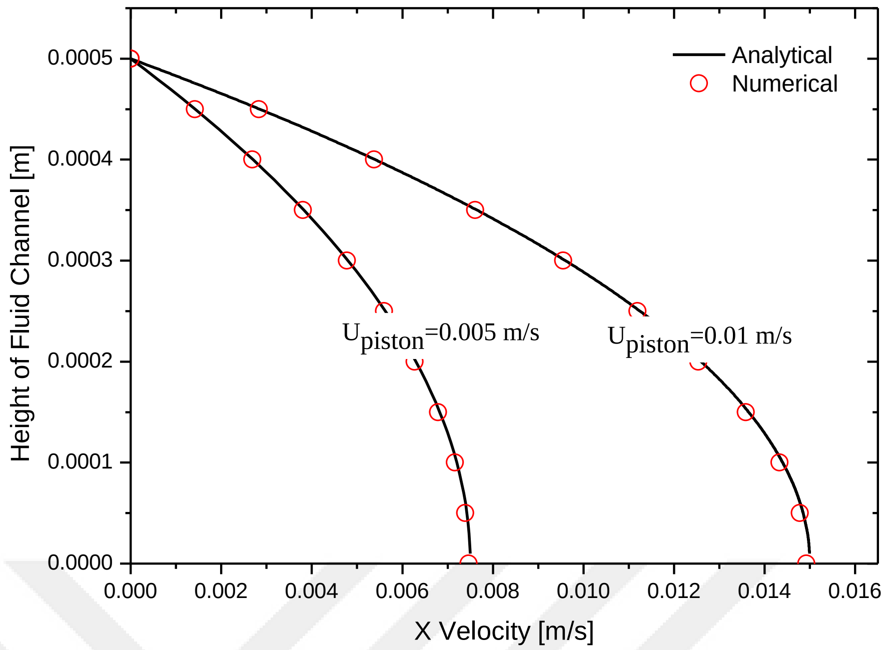

Figure 3.6 Hydrodynamic validation of parallel plate regenerator.

3.3.2 Effect of Piston Velocity

In the magnetic regenerator proposal, nine different piston velocities are considered as U_p=0.05 cm/s, U_p=0.075 cm/s, U_p=0.1 cm/s, U_p=0.125 cm/s, U_p=0.2 cm/s, U_p=0.15 cm/s, U_p=0.25 cm/s, U_p=0.03 cm/s, and U_p=0.35 cm/s. Different sets of piston velocities create different fluid displacement ratios. The displacement ratio indicates the fraction of the regenerator length that is swept during the hot blow or cold blow periods. In the literature, common approach to determine the performance of a magnetic regenerator is to obtain a dimensionless parameter called as utilization factor. Utilization factor is defined in Equation 3.8 (Ezan et al., 2017)

$$UF = \frac{\dot{m}_{HTF} c_{HTF} t_{flow}}{m_{gd} c_{gd}} \tag{3.8}$$

Here, $\dot{m}_{HTF}$ is heat transfer fluid’s mass flow rate in kg/s, c_{HTF} heat transfer fluid’s heat capacity is in Jkg^{-1}K^{-1}, t_{flow} is flow duration in the cycle in seconds (hot blow duration or cold blow duration), m_{gd} is magnetocaloric material’s mass in kg, c_{gd} is heat capacity of magnetocaloric material in $Jkg^{-1}K^{-1}$. Equation 3.8 is solved for every case and results are summarized in Table 3.4.

Table 3.4 Selected working parameters of parallel plate regenerator

Case	Piston Velocity [cm/s]	Utilization [-]	Displacement Ratio (%)
1	0.05	7.02E-02	10
2	0.075	1.05E-01	15
3	0.1	1.40E-01	20
4	0.125	1.76E-01	25
5	0.15	2.11E-01	30
6	0.2	2.81E-01	40
7	0.25	3.51E-01	50
8	0.3	4.21E-01	60
9	0.35	4.91E-01	70

In Figure 3.7, transient temperature variations are represented for every piston velocity. There is no cooling load at the CHEX and it is considered to be adiabatic in each case. It can be observed that increasing the piston velocity reduces the maximum temperature span between CHEX and HHEX.

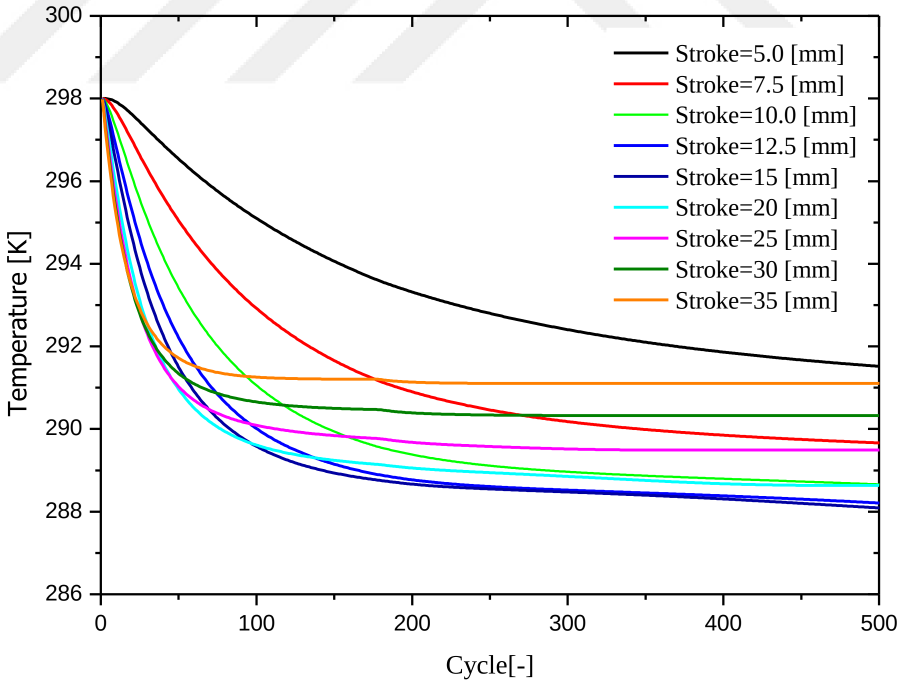

Figure 3.7 Temperature span by cycle at CHEX.

The maximum temperature span is observed approximately 9.9 K at the piston velocity of U_p=0.15 cm/s. It can be observed that the duration that is necessary for reaching the steady-state condition gets shorter with increasing the piston velocity. In conclusion, this result clarifies that increasing piston velocity causes lower temperature span values. Same results represented in the literature (Bahl, Petersen, Pryds & Smith, 2008; Ezan et al., 2017)

On the other hand, steady-state temperature span values are given with various fluid displacement ratios and as a function of increasing utilization factor in Figure 3.8.

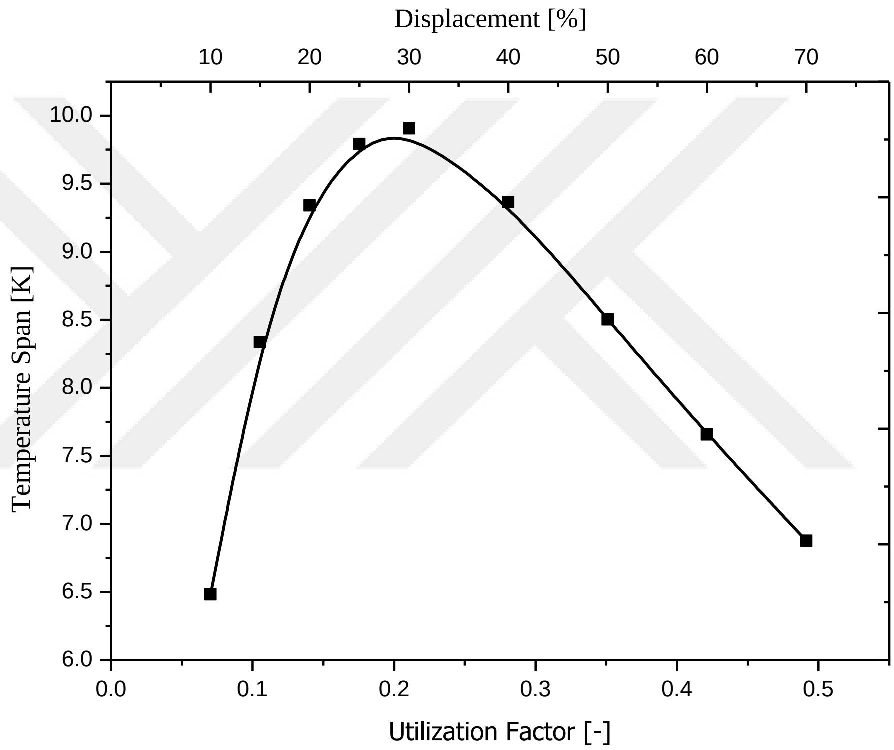

Figure 3.8 Temperature span by utilization factor and displacement ratio

Maximum temperature span value is observed for *UF* = 0.211 about 9.9 K. Beyond this value, the temperature span decreases. It can be said that for this parameter set and geometric configuration.

CHAPTER FOUR
CYLINDRICAL REGENERATOR

4.1 Definition of Problem

Proposed regenerator for magnetic cooling system consists of five essential components that are sufficient for numerical inputs, *(i)* cold water storage tank (CWST), *(ii)* hot water storage tank (HWST), *(iii)* magnetic regenerator (which includes cylindrical shaped magnetocaloric material), *(iv)* Halbach magnet array, and *(v)* pumps for circulating heat transfer fluid. System's operation is illustrated in Figure 4.1. As can be seen in Figure 4.1, the system operates in a cyclic manner, and steps of the cycle are named as (a) magnetization, (b) hot blow, (c) demagnetization, and (d) cold blow respectively.

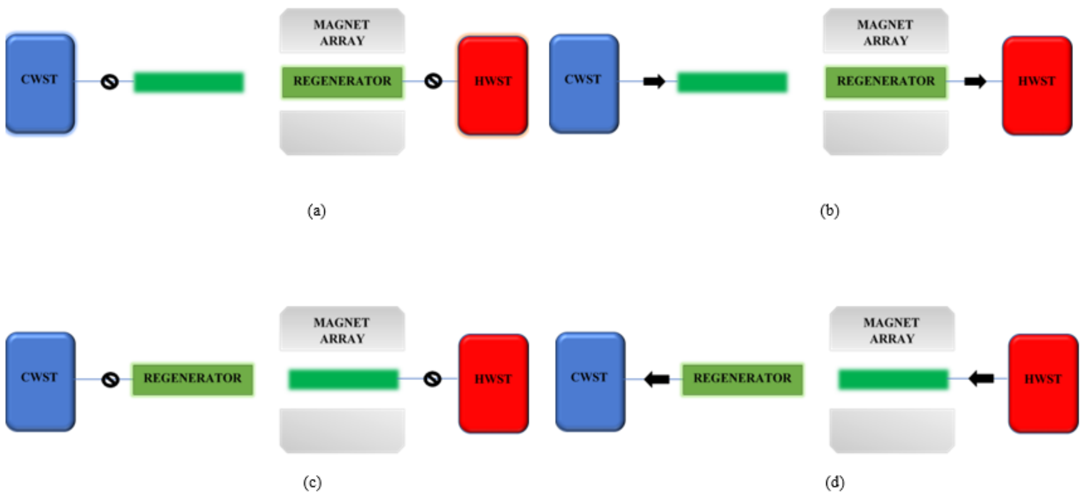

Figure 4.1 Schematic of the cyclic system, (a) Magnetization (b) Hot blow (c) Demagnetization (d) Cold blow

The physical build of the regenerator is illustrated in Figure 4.2. As can be seen in Figure 4.2, cylindrical Halbach array and cylindrical magnetocaloric material are positioned concentrically. Here $r, x,$ and ϕ represent radial, axial and azimuthal coordinates respectively. As illustrated in Figure 4.2, the physical model of regenerator has the axisymmetric condition and it allows dimensional reduction from 3D to 2D.

This reduction can reduce total mesh number and it provides shorter computational time without losing the accuracy.

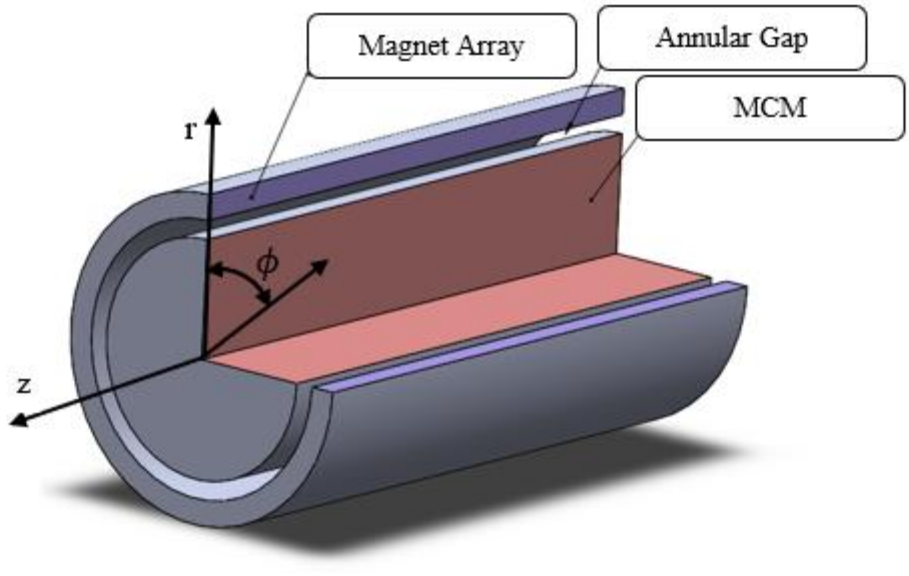

(a)

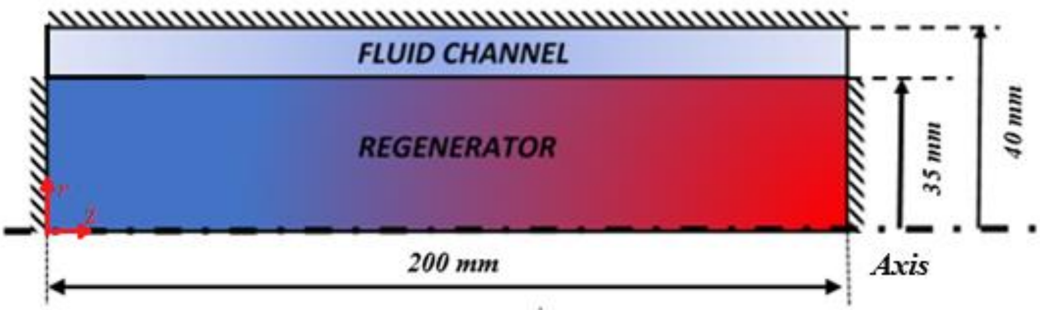

(b)

Figure 4.2 Physical build of cylindrical regenerator (a) 3-D model (b) Reduced 2-D model

In Figure 4.2(b), the reduced 2D numerical model can be seen with its boundary conditions. The dashed line represents the axisymmetric rotation axis. All patterned surfaces are assumed to be adiabatic. Also, geometric inputs are represented in Figure 4.2(b). This system works cyclically just as the parallel plate regenerator. First of all, magnetocaloric bed (or regenerator) runs into the Halbach array. Thus magnetocaloric material is magnetized, and its temperature increases, and then hot blow occurs. In this system, heat transfer fluid is circulated by a pair of pumps which are defined at the hot blow time or cold blow time. The heat transfer fluid is circulated by setting a pressure difference between each side of the fluid channel. This process should be performed with synchronous cyclic timing. So, when the right pump is started to work, the left pump should be closed. Thus, fluid flow occurs from the right side of the fluid channel to the left side of the fluid channel. After that, regenerator exits from the Halbach array, so magnetocaloric material is demagnetized, and its temperature decreases. Finally, the right pump is started to work, and an opposite flow, which is named as cold blow, occurs. The heat transfer fluid is stored inside separated tanks at the hot and cold sides of the system and re-circulated to the system by pumps. This cyclic process summarized in Figure 4.3.

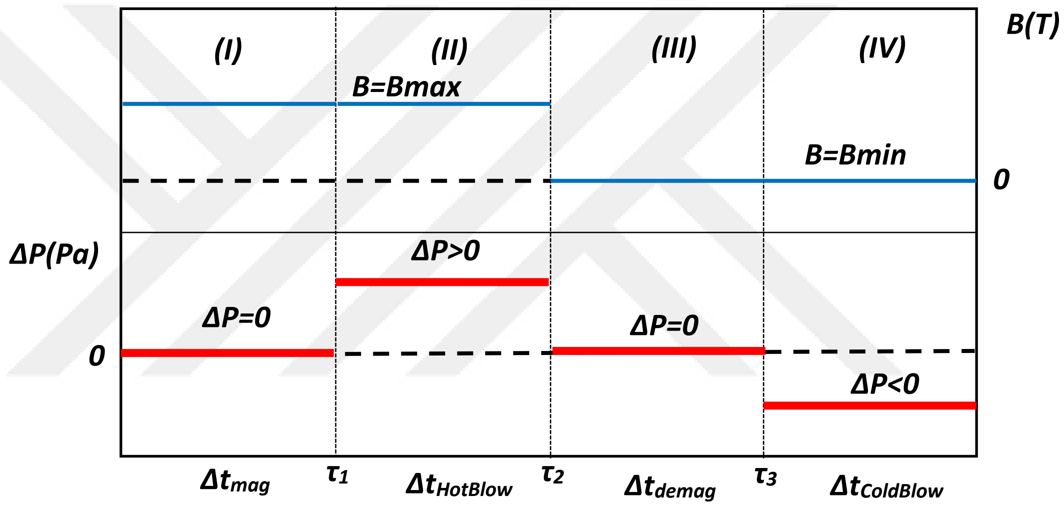

Figure 4.3 Cyclic process on cylindrical regenerator, (I) Magnetization (II) Hot Blow (III) Demagnetization (IV) Cold Blow

This magnetocaloric regenerator uses gadolinium (Gd) as magnetocaloric material since Gd's Curie temperature is near room temperature. Thermophysical properties of Gd were given in Section 3.1. The other thing is that Gd is magnetized by a Halbach cylinder which causes different magnetic field intensities as a function of position on solid domain. In Figure 4.4, magnetic field density variation along the axial direction of the regenerator is given. This magnetic field data employed from Yanik & Celik (2018). The variation along the radial direction is neglected due to the small gradient.

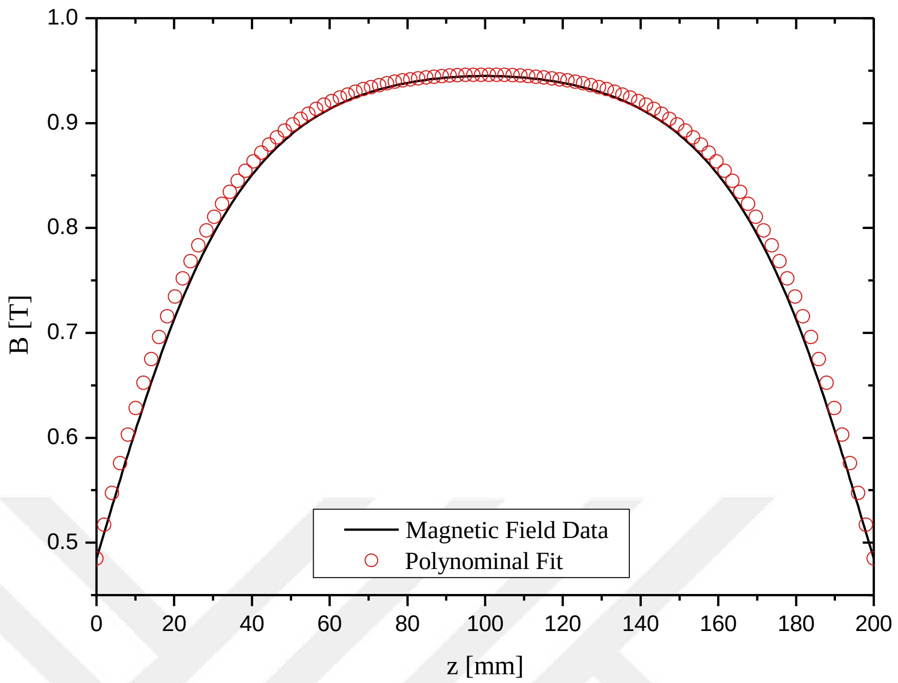

Figure 4.4 Magnetic field intensity along the axial direction of the regenerator

As discussed in Section 2.3, a UDF calculates the MCE. In this regenerator, magnetic flux density variation along the axial position is defined to the UDF as a fitted curve. A polynomial fit satisfies a function by axial distance as can be seen in Figure 4.4. The corresponding R^2 value is calculated as 0.99. This function and its parameters are given by Equation 4.1 and Table 4.1.

$$B(z) = A_0 + A_1 z + A_2 z^2 + A_3 z^3 + A_4 z^4 + A_5 z^5 \tag{4.1}$$

Table 4.1 Fitted magnetic field intensity curve values

Parameter	A_0	A_1	A_2	A_3	A_4	A_5
Value	0.48487	0.01632	-2.23E-04	1.42E-06	-3.55E-09	1.18E-24

In Figure 2.7, adiabatic temperature changes of magnetocaloric material are given by increasing magnetic field values. From Figure 4.4, one can see that the maximum magnetic field density value is observed as 1 T. The lowest value is nearly about 0.4 T. According to this magnetic field range, magnetocaloric material's adiabatic change is calculated between 0.4 T – 1.0 T with an increment of 0.1 T. As a simplification an interpolation is performed in the UDF to evaluate the intermediate values.

As illustrated in Figure 4.2(b) there are two main domains as (i) fluid channel (ii) regenerator. The left and right side of fluid channels are defined as pressure outlet boundary condition that simulates pumps in the system. All patterned sides are defined adiabatic, and the wall between the regenerator and the fluid channel is defined as a coupled wall to allow heat transfer.

The cylindrical regenerator is operated under two main branches of the parameter, one branch is various cycle durations and the other is different annular gap ratio. Each parameter branch is tested under pressure difference range of 5-120 Pa. Selected cycle durations are τ_{cycle} =1.2 s, τ_{cycle} =2.2 s, τ_{cycle} =4.2 s, τ_{cycle} =6.2 s. On the other hand, different Gd (or regenerator) diameters tested with one cycle duration τ_{cycle} =1.2 s under pressure difference range of 5-120 Pa. For determining this structural effect, a dimensionless ratio named as annular gap ratio is defined. This ratio was able to calculate from Equation 4.2.

$$K_{gap} = \frac{r_2}{r_1} \tag{4.2}$$

where r_2 is fluid channel radius and r_1 is Gadolinium diameter. K_{gap} is calculated by reducing gadolinium diameter 5mm in each step as 0.14, 0.60, and 1.00 respectively. Totally 68 analyses are performed and each of these analyses takes 44 hours under conditions.

4.2 Solution Method

Transient model is used for the present model solution. Several assumptions are made as follows

- Magnetic field density varies only along the axial direction of the regenerator. Radial changes are neglected
- The regenerator is ideally insulated, and only convective and conductive heat transfer mechanisms are active. Radiative heat transfer to the ambient is neglected.
- Heat capacity of magnetocaloric material is kept constant during the solution, but magnetic field intensity has an effect on heat capacity only for MCE contribution.
- Heat transfer fluid is incompressible
- Thermophysical properties of the fluid are kept constant during the solution.

For fluid domain, governing equations for 2-D axisymmetric geometries can be written as below (ANSYS-Fluent Theory Guide, n.d.). For the fluid domain, the continuity equation is given with Equation 4.3.

$$\frac{\partial}{\partial z}(\rho V_z) + \frac{\partial}{\partial r}(\rho V_r) + \frac{\rho V_r}{r} = 0 \tag{4.3}$$

Furthermore, axial and radial momentum equations are given with Equation 4.4 and Equation 4.5, respectively.

$$\begin{aligned}\frac{\partial}{\partial t}(\rho V_z) + \frac{1}{r}\frac{\partial}{\partial z}(r\rho V_z V_z) + \frac{1}{r}\frac{\partial}{\partial r}(r\rho V_r V_z) \\ = -\frac{\partial p}{\partial z} + \frac{1}{r}\frac{\partial}{\partial z}\left[r\mu\left(2\frac{\partial V_z}{\partial z} - \frac{2}{3}\left(\mathbf{\nabla}.\vec{V}\right)\right)\right] \\ + \frac{1}{r}\frac{\partial}{\partial r}\left[r\mu\left(\frac{\partial V_z}{\partial r} + \frac{\partial V_r}{\partial z}\right)\right]\end{aligned} \tag{4.4}$$

$$\frac{\partial}{\partial t}(\rho V_r) + \frac{1}{r}\frac{\partial}{\partial z}(r\rho V_z V_r) + \frac{1}{r}\frac{\partial}{\partial r}(r\rho V_r V_r) = -\frac{\partial p}{\partial r} + \frac{1}{r}\frac{\partial}{\partial r}\left[r\mu\left(2\frac{\partial V_r}{\partial r} - \frac{2}{3}(\nabla.\vec{V})\right)\right] + \frac{1}{r}\frac{\partial}{\partial z}\left[r\mu\left(\frac{\partial V_r}{\partial z} + \frac{\partial V_z}{\partial r}\right)\right] - 2\mu\frac{V_r}{r^2} + \frac{2}{3}\frac{\mu}{r}(\nabla.\vec{V}) \tag{4.5}$$

$$\nabla.\vec{V} = \frac{\partial V_z}{\partial z} + \frac{\partial V_r}{\partial r} + \frac{V_r}{r} \tag{4.6}$$

The energy equation for the fluid domain given with Equation 4.7.

$$\frac{\partial T_f}{\partial t} + \vec{V}\,\nabla T_f = \alpha_f\left(\nabla^2 T_f\right) \tag{4.7}$$

For solid domain, the axisymmetric 2-D energy equation is given with Equation 4.8.

$$\frac{\partial T_s}{\partial t} = \alpha_s(\nabla^2 T_s) + MCE \tag{4.8}$$

The second-order upwind scheme is implemented for the discretization of convective terms and energy equation. Continuity and momentum equations are solved with Semi-Implicit Method for Pressure-Linked Equations (SIMPLE) algorithm. MCE term's addition method is explained in Section 3.3. The same method is implemented here too. However magnetic field by along axial direction of the regenerator is computed by UDF. Because this type of regenerator configuration has various magnetic field intensity as a function of its axial direction.

Initially, the system is at the near room temperature (T_{amb} = 25 °C), and heat transfer fluid is stagnant (u = v = 0). Time step size is defined as 0.01 s for the transient point of view. Convergence criteria for all of governing equations set to be 10^{-6}.

Mesh independency is analyzed concerning gadolinium internal temperature. Three types of mesh build are tested for determining mesh independency. These three types of mesh cases are classified as a coarse mesh that has 6000 nodes, medium mesh that has 10800 nodes, and fine mesh that has 18200 nodes, respectively. Figure 4.5 represents results by mesh numbers.

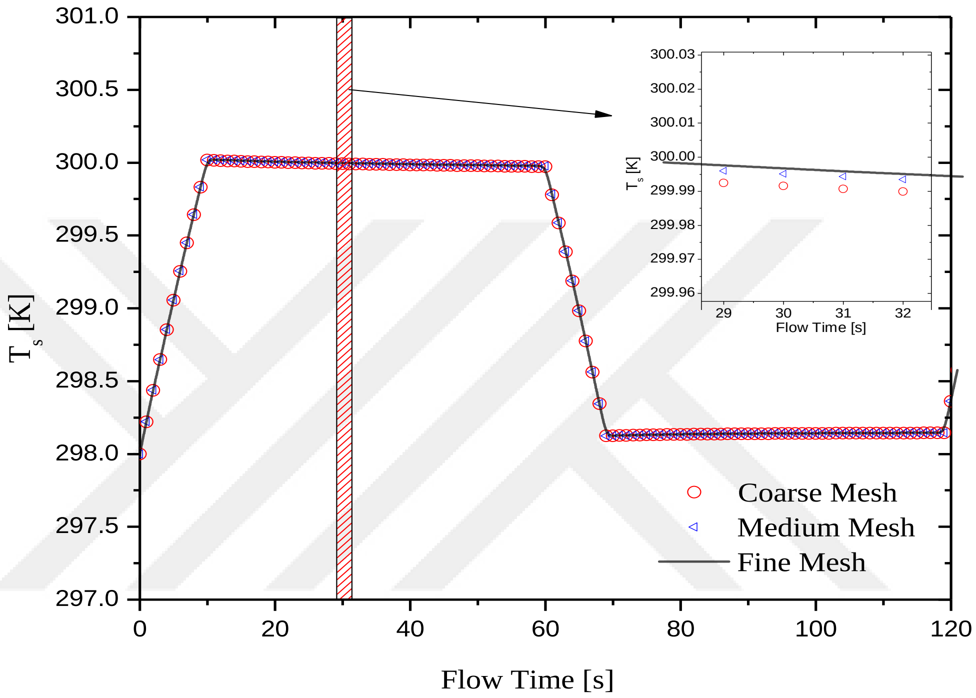

Figure 4.5 Mesh independency of the cylindrical regenerator

Coarse mesh reports that at a specific time, Gd internal volume average temperature is 299.78 K. If the same calculation is performed with fine mesh, calculated volume average temperature is observed as 299.99 K. Increasing mesh number from coarse to fine mesh size improves mesh quality 0.00174% and this improvement satisfies mesh quality.

4.3 Results of Cylindrical Regenerator

Numeric test results examined with two different branches, *(i)* hydrodynamical considerations, *(ii)* energetic considerations. Also, the behavior of magnetic cooling system and parameters that have vital influences on a magnetic regenerator explained more detailly at this section.

4.3.1 Hydrodynamic Considerations

The magnetocaloric regenerator is investigated hydrodynamically based on the pressure difference. Defined pressure difference provides fluid motion in this system. Axial velocity values are calculated at pressure outlets as area-weighted average. These values are cyclically averaged by an algorithm that developed in MATLAB. As an example, Figure 4.6 (a) shows this algorithm's result for τ_{cycle} = 1.2 s cycle duration and Δp = 5 Pa pressure difference. It has been observed that increasing cycle duration effects mean velocity value at the pressure outlets because increasing cycle durations gives more time to pumps for creating pressure difference. Figure 4.6(b) supports this observation with increasing positive slope of straight lines that represents mean velocity values by increasing pressure difference values.

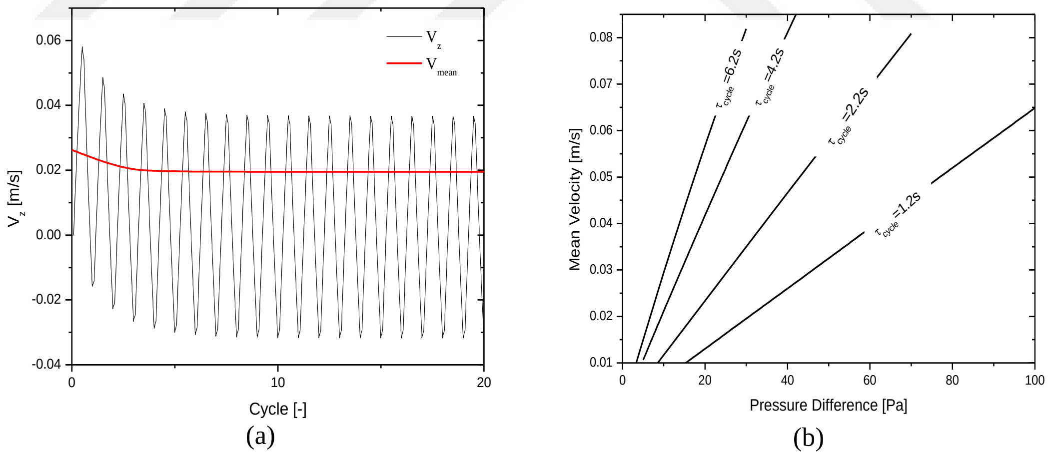

Figure 4.6 Mean velocity values by different pressure differences with increasing cycle durations (a) by cycle (b) by the Pressure difference

Also, there is Hagen-Poiseuille flow in the numerical domain. Fully developed velocity distribution under steady-state condition is validated with an analytical solution that can be seen in Figure 4.7.

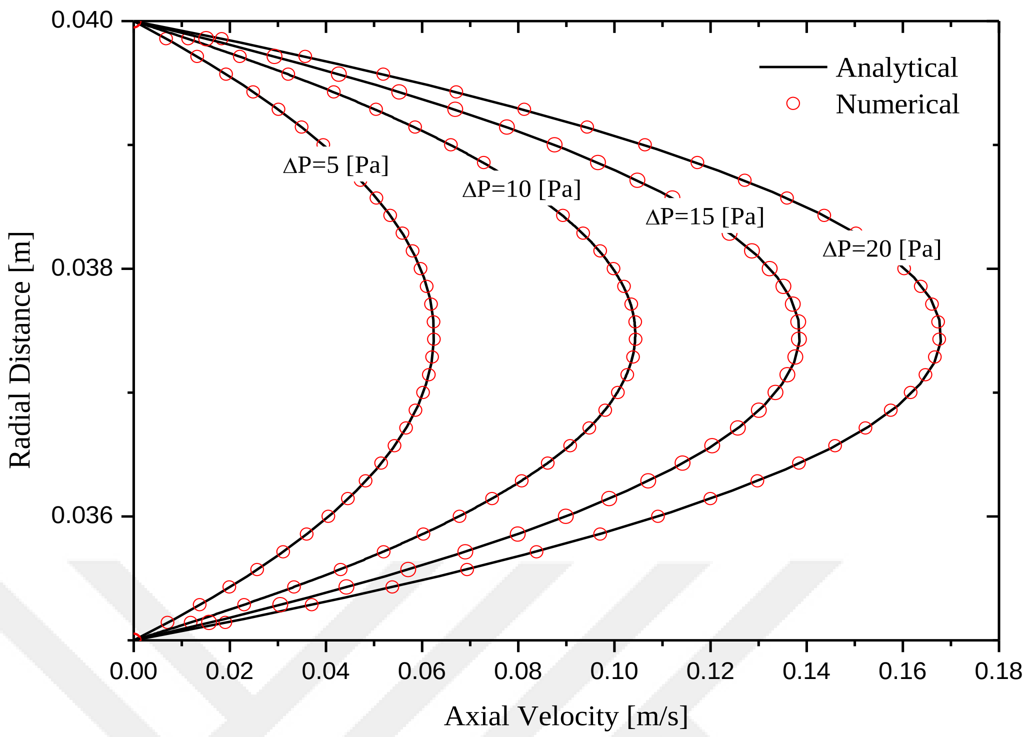

Figure 4.7 Validation of Hagen-Poiseuille flow for the cylindrical regenerator

4.3.2 Influence of Pressure Difference and Cycle Duration

In this section, energetic results are presented. Temperature span for each cycle durations can be found in Figure 4.8.

All temperature values are computed as the area-weighted average of the left side of the fluid channel that defined as the cold side. Calculated values are averaged with the developed MATLAB algorithm. For each cycle duration, steady-state condition is achieved with different times. Cold side temperature reaches steady state condition 350 cycles at τ_{cycle}=1.2 s (Figure 4.8(a)), 300 cycles at τ_{cycle}=2.2 s (Figure 4.8(b)), 250 at τ_{cycle}=4.2 s (Figure 4.8(c)), reaches 150 cycles at τ_{cycle}=6.2 s (Figure 4.8(d)). Under these observations, increasing cycle durations are reducing the time elapsed that is a need to be reaching steady state condition. This result is consistent with the literature (Bahl, Petersen, Pryds & Smith, 2008; Ezan et al., 2017)

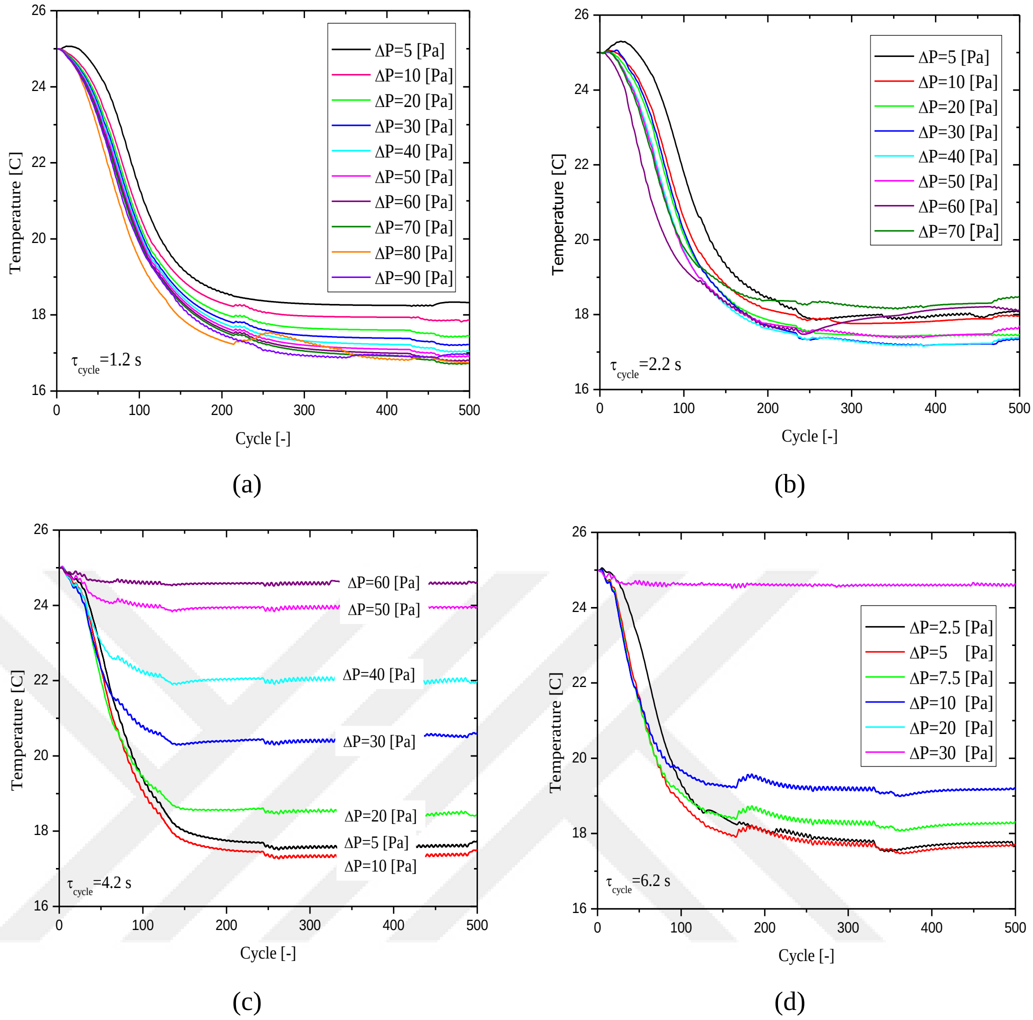

Figure 4.8 Temperature drops at cold side (a) τ_{cycle}=1.2 s, (b) τ_{cycle}=2.2 s, (c) τ_{cycle}=4.2 s, (d) τ_{cycle}=6.2 s

Temperature drops at the cold side of regenerator are summarized in Figure 4.9. It can be seen at Figure 4.9, the highest temperature spans are determined as ΔT_{span} = 8.28 K, ΔT_{span} = 7.63 K, ΔT_{span} = 7.47 K, ΔT_{span} = 7.28 K, with cycle durations τ_{cycle} = 1.2 s, τ_{cycle} = 2.2 s, τ_{cycle} = 4.2 s, τ_{cycle} = 6.2 s respectively. This result obviously shows that increasing cycle durations reduces highest temperature span values. Also, it can be inferred from Figure 4.9; long cycle durations reduce the working pressure difference ranges.

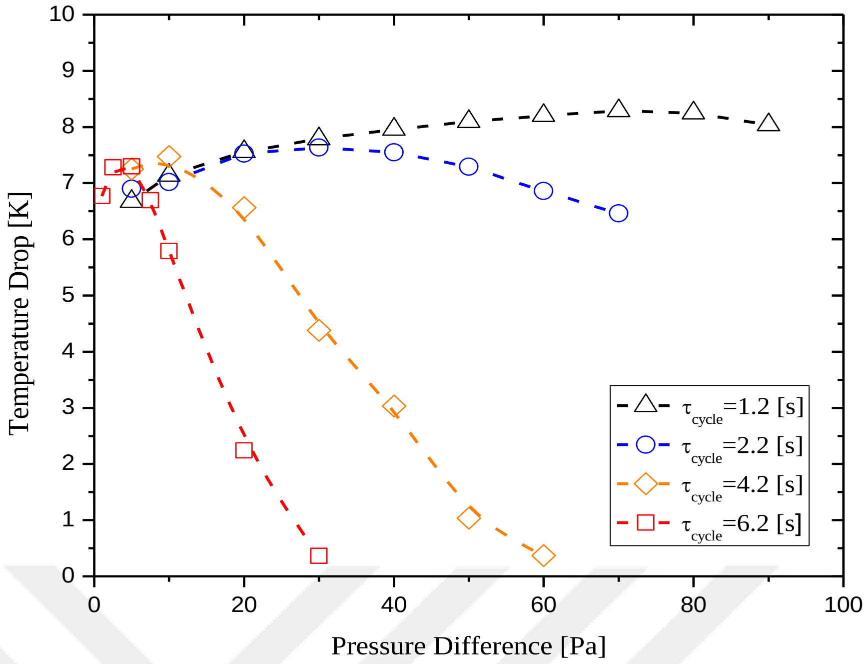

Figure 4.9 Temperature drops at the cold side with different cycle durations

Another thing is that the temperature gradient along the regenerator axial distance is examined for observing whether thermal stratification occurs in the regenerator or not. Also, this stratification creates a buffer zone between the cold side and hot side of the regenerator. In Figure 4.10, stratification is observed for three different pressure difference when τ_{cycle} = 2.2 s.

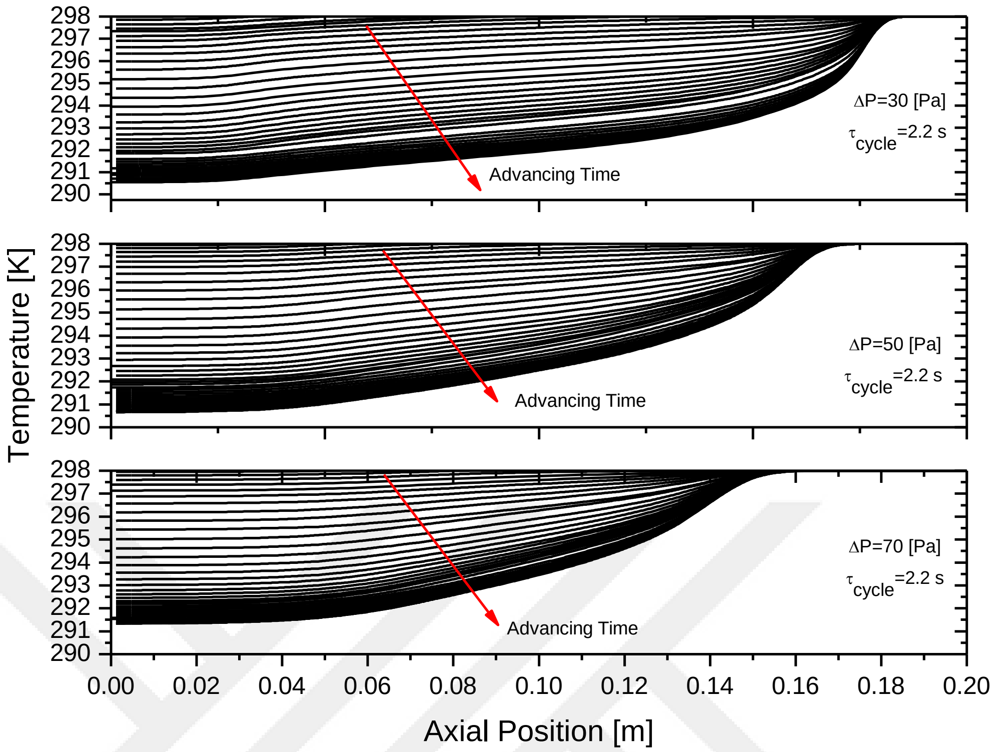

Figure 4.10 Thermal stratification development under various pressure differences

It is undesirable for the heat transfer fluid to be intermixed between the two ends of the flow channel, after being conditioned at the hot and cold end. Buffer region blocks intermixing so that this region's size is beneficial for regenerator performance. As can be seen in Figure 4.10, increasing pressure difference between both side of the fluid channel increases axial velocity as discussed in Section 4.3.1, thus increasing velocity shrinks the size of the buffer region. This result is consistent with the literature (Roadaut, Kedous-Lebouc, Yonnet & Muller, 2011) On the other hand; increased cycle duration shows the same effect because this increment accelerates fluid in the axial direction. This situation is represented in Figure 4.11.

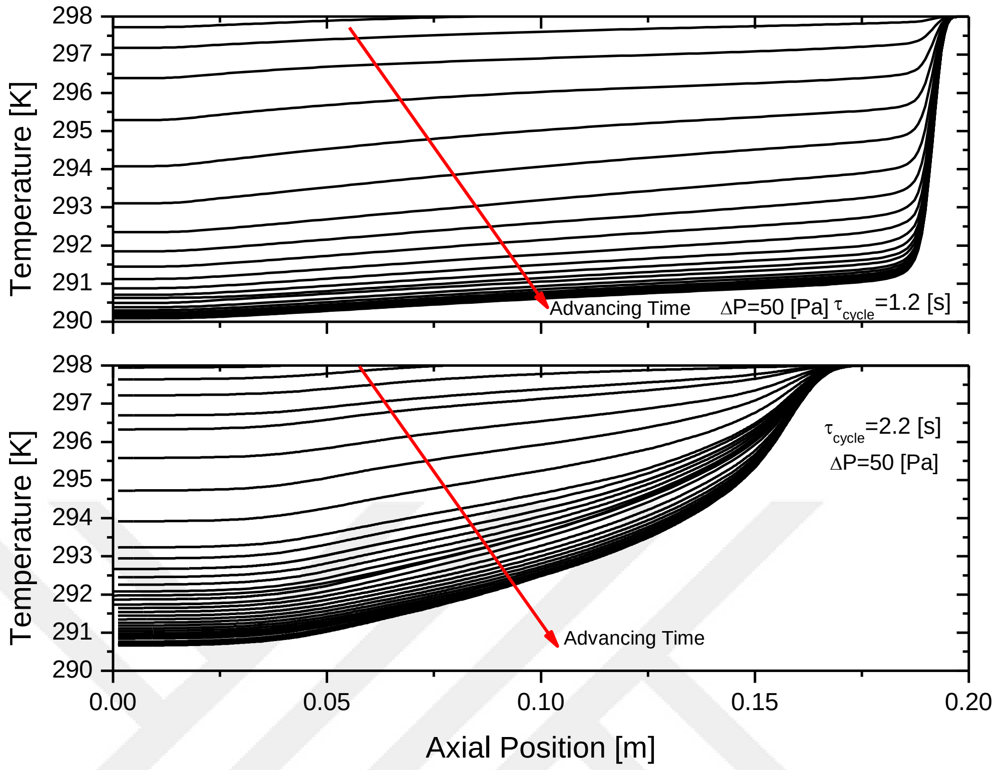

Figure 4.11 Thermal stratification development under various cycle durations.

For each cycle duration, maximum temperature span value is determined for τ_{cycle}=2.2 s at *UF*=0.0782 as ΔT_{span}=8.28 K. It is observed that after this *UF* value, temperature span values reduce by increasing *UF* values. Temperature drop values by *UF* for each cycle duration is represented in Figure 4.12. It can be observed that temperature drop curves overlap each other and almost becomes independent from cycle durations. This result explains why we adopted a dimensionless number called as *UF*. Thus one can clearly obtain the best-operating conditions of a magnetic regenerator. *UF* calculations are already defined in-detail in Section 3.3.2. Time of heat transfer between the fluid and the Gd increases as reducing the velocity of the heat transfer fluid, the outlet temperature of the HTF approaches to the Gd temperature for slow fluid velocity values. The highest temperature span of regenerator (smaller duration times) is observed at the highest fluid velocity.

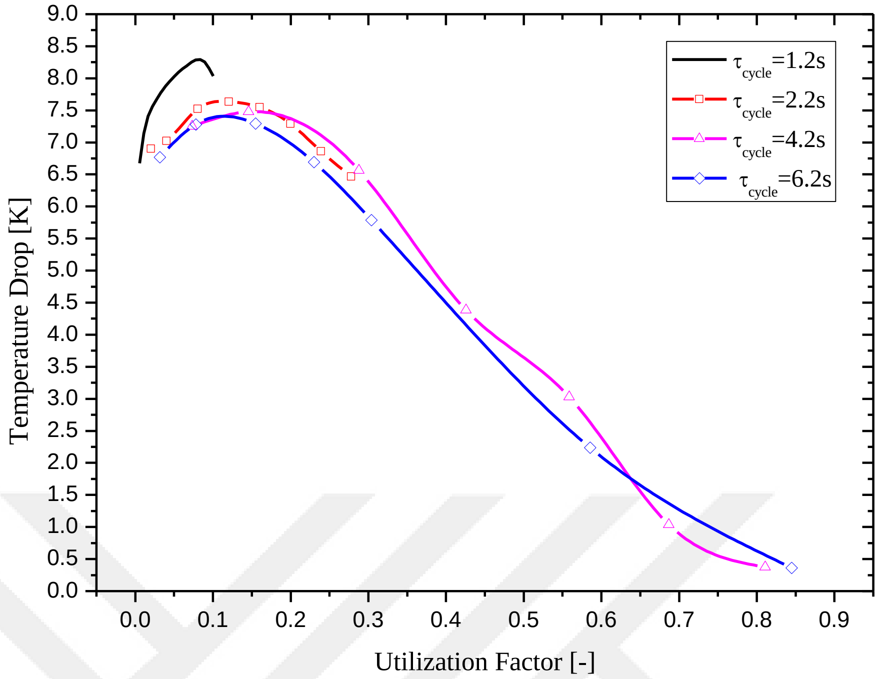

Figure 4.12 Temperature drops at the cold side of cylindrical regenerator by the utilization factor

4.3.3 Influence of Annular Gap

The regenerator is studied with a structural point of view in this section. Temperature drop at the cold side of the regenerator is represented in Figure 4.13. Here it can be seen that smaller Gd diameter provides more temperature span between the cold side and hot side of the regenerator. This increment at temperature span could be explained with the volume of the Gd. Smaller diameters provide smaller volumes, so the interaction between heat transfer fluid and Gd is expanded; thus heat transfer mechanism between heat transfer fluid and magnetocaloric material is improved.

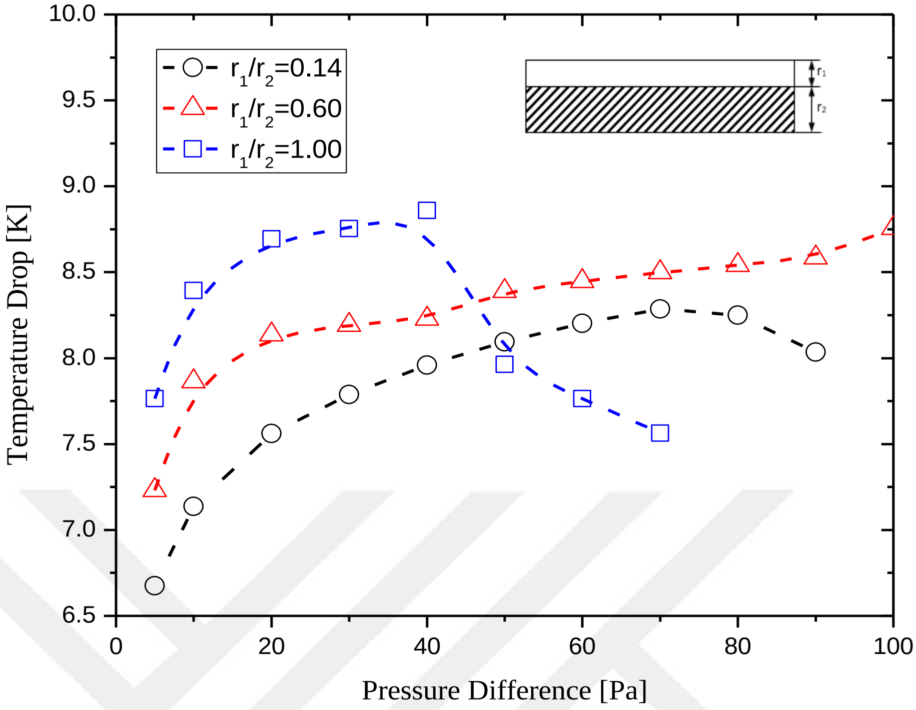

Figure 4.13 Temperature drops at the cold side of cylindrical regenerator by increasing pressure differences and different annular gap ratios

In Figure 4.13, the maximum temperature drops for K_{gap}=0.14, K_{gap}=0.60, K_{gap}=1.00, obtained as ΔT_{span}=8.28 K, ΔT_{span}=8.75 K, ΔT_{span}=8.85 K respectively. Also, efficient operating pressure difference range is improved for K_{gap}=0.60 as can be seen in Figure 4.13. Sudden temperature drop at the cold side of regenerator observed for K_{gap}=1.00 after 40 Pa pressure difference. One of the important findings observed is that the heat transfer fluid accelerating with decreasing volume of gadolinium causes such a sudden drop. This can be explained by the low heat transfer coefficient of gadolinium and the independence of the solution from the lumped analysis.

CHAPTER FIVE
CONCLUSIONS

In the current thesis, two types of magnetocaloric regenerator are proposed and solved numerically. In addition, two different MCE solution method are investigated. MCE is included in the energy equation as a source term. To do so, a user-defined function (UDF) is developed in C language for each type of regenerator. After this integration, each regenerator type is investigated by hydrodynamical point of view, beyond that energetic performances are studied with MCE by commercial CFD solver ANSYS-FLUENT. For the parallel plate regenerator, it is observed that

- Hydrodynamic behavior of the system is consistent with its analytical solution. This situation shows that laminar flow assumption is valid for this regenerator geometry. Also, mesh independency is observed with this result.
- At piston velocity of U_p=0.15 cm/s maximum temperature drop at cold heat exchanger is observed as 9.9 K and corresponding utilization factor and fluid displacement ratio are 0.211 and 25%, respectively.

The cylindrical regenerator is examined in the same manner with parallel plate regenerator. All hydrodynamic and energetic stages are implemented as parallel plate exchanger's solution stages. Key parameters for cylindrical regenerator are cycle duration, the pressure difference between left and right sides of the fluid channel, annular gap ratio, and corresponding utilization factor.

According to observed results for cylindrical regenerator, it is concluded that

- Hydrodynamic behavior of regenerator is validated with its analytical solution. This behavior is the same with Hagen- Poiseuille flow because of the regenerator geometry. It is observed that increasing cycle duration causes an increment in mean velocity at the exit of the fluid channel. This increment affects directly maximum temperature value at the cold side of the regenerator.
- Increasing cycle duration has an adverse effect on the thermal performance of the magnetic refrigeration system. On the other hand, increasing cycle duration

shrinks the buffer region that is the result of thermal stratification. This shrinkage also has a negative effect on the regenerator performance.

- Temperature drop values are presented as a function of the utilization factor (*UF*). As an interesting result, it is concluded that temperature span curves become almost independent from the cycle duration. Thus ideal operating conditions under different cycle durations are determined at *UF*=0.0782 as ΔT_{span}=8.28 K for cylindrical regenerator.
- From a structural point of view, smaller Gd diameters provide higher temperature drop at the cold side of the regenerator. Also, this diameter reduction expands operating pressure difference range of regenerator.
- Temperature drop that is observed in the parallel plate regenerator is 19.56% higher than the cylindrical one. However, it should be noted that the cylindrical regenerator operates in a wider operating pressure range and therefore, in the fluid velocity range.

REFERENCES

Aprea, C., Greco, A., & Maiorino, A. (2016). Magnetic refrigeration: a promising new technology for energy saving. *International Journal of Ambient Energy*, *37*(3), 294-313.

Aprea, C., Greco, A., & Maiorino, A. (2017). An application of the artificial neural network to optimise the energy performances of a magnetic refrigerator. *International Journal of Refrigeration, 82*, 238-251.

Aprea, C., Greco, A., Maiorino, A., & Masselli, C. (2015). A comparison between rare earth and transition metals working as magnetic materials in an AMR refrigerator in the room temperature range. *Applied Thermal Engineering*, *91*, 767-777.

Bahl, C. R. H., Petersen, T. F., Pryds, N., & Smith, A. (2008). A versatile magnetic refrigeration test device. *Review of Scientific Instruments*, *79*(9), 093906.

Bouchekara, H. R. E. H., & Nahas, M. (2012). Magnetic refrigeration technology at room temperature. Barsan V., & Lungu R.P. (Ed.), *Trends in electromagnetism-from fundamentals to applications* (1st ed.) (226-251), Croatia: Intechopen.

Brown, G. V. (1976). Magnetic heat pumping near room temperature. *Journal of Applied Physics*, *47*(8), 3673-3680.

De Almeida, A. T., Fonseca, P., Falkner, H., & Bertoldi, P. (2003). Market transformation of energy-efficient motor technologies in the EU. *Energy Policy*, *31*(6), 563-575.

Engelbrecht, K. L., Nellis, G. F., & Klein, S. A. (2005). A numerical model of an active magnetic regenerator refrigeration system. In *Cryocoolers 13* (471-480). Boston, MA: Springer US.

Eriksen, D., Engelbrecht, K., Bahl, C. R. H., Bjørk, R., Nielsen, K. K., Insinga, A. R., & Pryds, N. (2015). Design and experimental tests of a rotary active magnetic regenerator prototype. *International Journal of Refrigeration*, *58*, 14-21.

Eriksen, D., Engelbrecht, K., Bahl, C.R.H., Bjork, R., Nielsen, K.K. (2016). Effects of flow balancing on active magnetic regenerator performance. *Applied Thermal Engineering, 103*, 1–8.

Ezan, M. A., Ekren, O., Metin, C., Yilanci, A., Biyik, E., & Kara, S. M. (2017). Numerical analysis of a near-room-temperature magnetic cooling system. *International Journal of Refrigeration*, *75*, 262-275.

Giauque, W. F. (1927). A thermodynamic treatment of certain magnetic effects. A proposed method of producing temperatures considerably below 1 absolute. *Journal of the American Chemical Society*, *49*(8), 1864-1870.

Goetzler, W., Guernsey, M., Young, J., Fuhrman, J., & Abdelaziz, O. (2016). *The future of air conditioning for buildings*. US Department of Energy, Energy Efficiency & Renewable Energy, Building Technologies Office.

Kamran, M.S., Sun, J., Tang, Y.B., Chen, Y.G., HongWu, J., ShengWang, H. (2016). Numerical investigation of room temperature magnetic refrigerator using microchannel regenerators. *Applied Thermal Engineering*, *102*, 1126–1140.

Kusiak, A., Li, M., & Tang, F. (2010). Modeling and optimization of HVAC energy consumption. *Applied Energy*, *87*(10), 3092-3102.

Lei, T., Engelbrecht, K., Nielsen, K.K., Veje, C.T. (2017). Study of geometries of active magnetic regenerators for room temperature magnetocaloric refrigeration. *Applied Thermal Engineering*, *111*, 1232-1243.

Lionte, S., Vasile, C., & Siroux, M. (2015). Numerical analysis of a reciprocating active magnetic regenerator. *Applied Thermal Engineering*, *75*, 871-879.

Lozano, J., Engelbrecht, K., Bahl, C., Nielsen, K., Eriksen, D., Olsen, U., Pryds, N. (2013). Performance analysis of a rotary active magnetic refrigerator. *Applied Energy, 111*, 669-680.

Niknia, I., Campbell, O., Christiaanse, T.V., Govindappa, P., Teyber, R., Trevizoli, P.V.,& Rowe, A. (2016). Impacts of configuration losses on active magnetic regenerator device performance. *Applied Thermal Engineering, 106*, 601-612.

Petersen, T. F. (2007). *Numerical modelling and analysis of a room temperature magnetic refrigeration system.* Phd Thesis, Fuel Cells and Solid State Chemistry Department, Technical University of Denmark, Roskilde.

Protocol, M. (1987). Montreal protocol on substances that deplete the ozone layer. *Washington, DC: US Government Printing Office, 26*, 128-136.

Qian, S., Geng, Y., Wang, Y., Ling, J., Hwang, Y., Radermacher, R., & Cui, J. (2016). A review of elastocaloric cooling: materials, cycles and system integrations. *International Journal of Refrigeration*, *64*, 1-19.

Roudaut, J., Kedous-Lebouc, A., Yonnet, J. P., & Muller, C. (2011). Numerical analysis of an active magnetic regenerator. *International Journal of Refrigeration, 34*(8), 1797-1804.

Strecka, J. (2015). *A brief account of the Ising and Ising-like models: Mean-field, effective-field and exact results*. Retrieved November 10, 2015, from https://arxiv.org/abs/1511.03031

Theory Reference ANSYS release 16.2.3 (n.d.). Retrieved April 9, 2019, from https://www.sharcnet.ca/Software/Ansys/16.2.3

Tishin, A. M. (1990). Magnetocaloric effect in strong magnetic fields. *Cryogenics*, *30*(2), 127-136.

Velázquez, D., Estepa, C., Palacios, E., & Burriel, R. (2016). A comprehensive study of a versatile magnetic refrigeration demonstrator. *International Journal of Refrigeration*, *63*, 14-24.

Weiss, P., & Piccard, A. (1917). Le phénomène magnétocalorique. *Journal of Physics: Theories and Applications*, *7*(1), 103-109.

Yanik, E., & Celik, S. (2018). Analysis of Magnetic Refrigeration Designs with Three Different Magnet Array Geometries. *ASHRAE Transactions*, *124*(1), 12-21.

Yu, B. F., Gao, Q., Zhang, B., Meng, X. Z., & Chen, Z. (2003). Review on research of room temperature magnetic refrigeration. *International Journal of Refrigeration*, *26*(6), 622-636.

APPENDICES

A. Nomenclature

T	Cell temperature, K
c	Heat capacity, $Jkg^{-1}K^{-1}$
t	Time, s
B	Magnetic field density, T
J	Spin angular momentum
g_j	Spectroscopic factor
K	Boltzmann constant
$S_{magnetic}$	Magnetic Entropy, $Jkg^{-1}K^{-1}$
$S_{lattice}$	Lattice Entropy, $Jkg^{-1}K^{-1}$
$S_{electron}$	Electron Entropy, $Jkg^{-1}K^{-1}$
S	Entropy, $Jkg^{-1}K^{-1}$
V	Velocity, ms^{-1}
R_u	Universal gas constant
r_1, r_2	Outer, Inner radius

Subscripts

Total, tot	Total of a quantity
ad	adiabatic
Curie	Curie value of a quantity
Debye	Debye value of a quantity
x	x-direction
y	y-direction
z	Axial direction
r	Radial direction

Greek Symbols

ρ	Density, kgm^{-3}
μ_b	Bohr magneton
μ	Dynamic viscosity, $kgm^{-1}s^{-1}$
α	Thermal diffusivity, m^2s^{-1}

Acronyms

MCE	Magnetocaloric effect
UDF	User-defined function
MCM	Magnetocaloric material
CHEX	Cold heat exchanger
HHEX	Hot heat exchanger
CWST	Cold water storage tank
HWST	Hot water storage tank
UF	Utilization factor